In search of synergy: novel therapy for metastatic uveal melanoma

Glinkina, K.A.

Chapter

2

PRECLINICAL EVALUATION OF TRABECTEDIN IN COMBINATION WITH TARGETED INHIBITORS FOR TREATMENT OF METASTATIC UVEAL MELANOMA

Kseniya Glinkina[1], Fariba Nemati[2], Amina F.A.S. Teunisse[1], Maria Chiara Gelmi[3], Vesnie Etienne[2], Muriel J. Kuipers[1], Samar Alsafadi[4], Martine J. Jager[3], Didier Decaudin[2,5], Aart G. Jochemsen[1]

1. Department of Cell and Chemical Biology, Leiden University Medical Center, Leiden, The Netherlands
2. Laboratory of Preclinical Investigation, Department of Translational Research, Institut Curie, PSL University, Paris, France
3. Department of Ophthalmology, Leiden University Medical Center, Leiden, The Netherlands
4. Uveal Melanoma Translational Group, Department of Translational Research, Institut Curie, PSL Research University, Paris, France
5. Department of Medical Oncology, Institut Curie, Paris, France

Published in *Invest Ophthalmol Vis Sci* 2022, 63(13): 14.

Abstract

Purpose: Uveal melanoma (UM) is considered a rare disease, yet it is the most common intraocular malignancy in adults. The primary tumor may be efficiently managed, nevertheless more than 50% of the UM patients develop distant metastases. The mortality at the first year after diagnosis of metastatic UM has been estimated at 81%, and the poor prognosis has not improved in the past years due to lack of effective therapies.

Methods: In order to search for novel therapeutic possibilities for metastatic UM, we performed a small-scale screen of targeted drug combinations. We verified the targets of the tested compounds by Western blotting and PCR and clarified the mechanism of action of the selected combinations by caspase 3/7 activity assay and flow cytometry. The best two combinations were tested in a mouse PDX UM model as putative therapeutics for metastatic UM.

Results: The combinations of the multitarget drug Trabectedin with either the CK2/Clk double-inhibitor Silmitasertib or with the c-MET/TAM (TYRO3, AXL, MERTK) receptor inhibitors Foretinib and Cabozantinib demonstrated synergistic effects and induced apoptosis (the relative caspase 3/7 activity increased up to 20.5-fold in UM cell lines). In case of Foretinib/Cabozantinib, inhibition of the TAM receptors, but not c-Met was essential to inhibit the growth of UM cells. Monotreatment with Trabectedin inhibited the tumor growth by 42%, 49%, and 35% in the MM26, MM309, and MM339 PDX mouse models, respectively.

Conclusion: Trabectedin alone or in combination with Cabozantinib inhibits the tumor growth in PDX UM mouse models. Blocking of MERTK, rather than TYRO3 activity inhibits UM cell growth and synergizes with Trabectedin.

Introduction

Uveal Melanoma (UM) is a malignant tumor that arises from the melanocytes located in the uveal tract of the eye. Uveal melanoma is considered a rare disease with the incidence of 2-8 cases per million per year in Europe [1], yet it is the most common intraocular malignancy in adults. The primary tumor may be efficiently managed by the local therapy, nevertheless more than 50% of the UM patients develop distant metastases. UM metastases are in most cases restricted to the liver; other metastatic sites are lungs, skin, brain, thyroid and colon [2]. Metastatic UM is very aggressive, as the mortality at the first year after diagnosis reaches 81% [3].

The poor prognosis for metastatic UM patients has not improved in the past years due to lack of effective novel therapies. One established local treatment option for hepatic metastases is isolated liver perfusion with a chemotherapeutic agent melphalan. The response rate to this therapy is reported to be higher than 50% with significant regression of the lesions. However only a restricted cohort of the patients is eligible, metastases recurrence after the isolated liver perfusion is frequent, also the procedure is complex and potentially associated with morbidity [4-7].

The numerous recently conducted clinical trials for metastatic UM resulted in limited improvement of the overall survival [8]. Among the tested drugs were chemotherapeutics such as dacarbazine (alone or in combination with MEK inhibitor selumetinib), and fotemustine [9, 10] and some targeted therapeutics such as the MEK inhibitor trametinib [11], the tyrosine kinase inhibitor imatinib [12], and the HSP90 inhibitor ganetespib [13]. Immunotherapeutic targeting of PD-1, recognized as a promising option for metastatic cutaneous melanoma, has demonstrated no effect on overall survival of the patients with metastatic UM, with the exception of UM with MBD4 mutation and increased mutation load [14, 15]. At present, the only approved systemic treatment is Tebentafusp - a bi-specific protein able to bind simultaneously to the gp100-HLA-A*02:01 complex on UM cells and CD3 on the T-cell membrane, thus redirecting the T cells towards UM cells. The phase 3 trial of Tebentafusp in HLA-A*02:01–positive metastatic UM patients delivered encouraging results. Overall survival at 1 year was 73% in the treatment group and 59% in the control group, while progression-free survival also increased significantly [16].

Commonly, UM has relatively low mutation burden [17, 18]. The most recurrent alterations (more than 90% of all cases) are the activating mutations in the genes *GNAQ* or *GNA11* encoding the G-proteins Gαq and Gα11, respectively [19]. The activating mutations in G-protein coupled receptor *CYSLTR2* or in signal mediator *PLCB4* are detected in the remaining UM cases [20, 21]. The constant activity of the Gα-proteins signaling cascade leads to dysregulation of multiple downstream effectors such as PKC, MAP kinases and YAP1 and causes uncontrolled proliferation of UM cells [22, 23]. Besides the somatic mutations in *GNAQ* and *GNA11*, UM is characterized by copy number variation of the chromosomes 1q, 3, 6p, 8q [24-27]. Amplification of chromosome 8q and, especially, loss of chromosome 3, are strong prognostic factors for metastasis. Chromosome 3 carries the *BAP1* gene, encoding a ubiquitin hydrolase. *BAP1* is frequently found mutated in the remaining allele in UM with monosomy 3, what leads to complete loss of BAP1 expression and strongly correlates with metastases development and poor prognosis [28]. Other factors of metastatic risk are the mutations in splicing modulators *SF3B1* and *SRSF2* [19]. The mutation in the translation initiation factor *EIF1AX*, on the contrary, correlates with disomy of chromosome 3 and low risk of metastases [29].

The absence of a targetable strong driver mutation may be one of the reasons for single

agent treatments to be ineffective for UM. The mutations in *GNAQ/11* lead to imbalance in the wide signaling landscape instead of activating one specific pathway and currently these mutant G-proteins cannot be selectively inhibited, although depsipeptides FR900359 and YM-254890 show promising results in preclinical experiments [30]. Therefore, combining several therapeutic agents targeting distinct signaling pathways might be beneficial as it allows suppressing multiple signaling cascades. In this work we have focused on examining the effect of dual combinations of several targeted compounds on the viability of UM cell lines, either derived from UM metastases, or with the genetic background that corresponds to metastases predisposition. We have performed a small-scale drug screen of the four agents – Trabectedin (Yondelis), Foretinib, CX-4945 (Silmitasertib) and RG7112 - and their combinations on a panel of 7 UM cell lines (The characteristics of the compounds are summarized in Table 1; the genetic aberrations of the UM cell lines are described in Table 2). These agents target the pathways reported to be important for growth or metastatic spread of UM [31-35]. Our results show that the combinations of Trabectedin with either CX-4942 or Foretinib (at later stages replaced by Cabozantinib) efficiently inhibit the growth of UM cells in cell culture and could be considered as putative therapeutics for metastatic UM.

Results

Identification of the synergistic combinations

We performed a screen of the dual combinations of the following inhibitors: Trabectedin, Foretinib, CX-4945 and RG7112 (Table 1), on a panel of 7 uveal melanoma cell lines, derived either from UM metastases or from primary tumors not expressing BAP1, a strong factor for poor prognosis (Table 2).

We assessed the effect of the drug combinations on the cell viability after 5 days of the treatment; based on the effect matrix, we calculated the synergistic score of the combinations using Excess over Bliss model [45] (Suppl Fig. 1A). Fig. 1A represents the matrix of the highest calculated Excess over Bliss score of each treatment per cell line. The combinations of RG7112 either demonstrated low Excess over Bliss values (RG7112 with Foretinib) or were synergistic only in a subset of the cell lines (RG7112 with Trabectedin or CX-4945), while the combinations of CX-4945 with Foretinib, or of Trabectedin with either CX4945 or Foretinib, showed the positive synergistic scores across most of the tested cell lines. Figures 1B, 1C and Supplementary figures 1B-E illustrate the effect of Trabectedin combined with either CX-4945 or Foretinib on survival of UM cell lines. It is worth noting that all the tested UM cell lines are sensitive to

Table 1. The drugs included into the screen

Drug	Target/ Mechanism of action	Clinical trials phase
Trabectedin	RNA Pol II, DNA-bound proteins, tumor microenvironment/ Multitarget DNA-damaging agent	3
CX-4945	Casein Kinase 2, Cyclin-like kinases	1-2
Foretinib	C-Met, VEGFR2, TAM (Tyro, AXL, MERTK) receptors	2
RG7112	MDM2-p53 interaction/ p53 activator	1

Table 2. Uveal melanoma cell lines included into the screen.

Cell Line	Origin	GNAQ Mutation	GNA11 Mutation	BAP1 Expression
OMM2.3	Liver metastases	c.626 A > C	-	Yes
OMM2.5	Liver metastases	c.626 A > C	-	Yes
OMM1	Subcutaneous metastasis	-	c.626 A > T	Yes
MM66	PDX established from liver metastasis	-	c.626 A > T	Yes
MM28	PDX established from liver metastasis	-	c.626 A > T	No
MP46	PDX established from primary tumor	c.626 A > T	-	No
MP38	Primary tumor	c.626 A > T	-	No

Trabectedin in picomolar concentrations.

The combinations of Trabectedin with either CX-4945 or Foretinib reduced the survival of the cells more effectively than either of the single treatments, and less than 10% of the cells were viable at the highest tested concentrations after 5 days of treatment. Taking into account the significant effect of the combinations on cell survival and the high synergy scores, we chose the combinations CX-4945 with Foretinib, or Trabectedin with either CX-4945 or Foretinib for further investigation.

The combination of Trabectedin with either CX-4945 or Foretinib stimulates apoptosis in UM cell lines

Next, we decided to examine the mechanism of action of the selected drug combinations. We assayed the activity of caspases 3 and 7 to clarify whether the selected combinations induce apoptosis (Fig. 1D-F). The caspase 3/7 activity rose less than 2-fold in case of treatment with either Foretinib or CX-4945, while it showed variable increase from 1.1 fold in OMM1 to 7.9 fold in MM66 upon Trabectedin treatment. In general, the effect of the combination Foretinib-CX-4945 was less pronounced than the effect of the combinations of Trabectedin with either Foretinib or CX-4945. The combination Foretinib-CX-4945 (Fig. 1D) increased caspase activity in MP38 (4-fold), MP46 (2.6-fold) and MM66 (6.5-fold). The combination of Trabectedin with either CX-4945 (Fig. 1E) or Foretinib (Fig. 1F) strongly activated caspases 3/7 in most of the tested cell lines. The highest effect was observed in the combination Trabectedin-Foretinib: the relative caspase 3/7 activity increased 5 times in OMM2.5, 9.2 times in MP38 and 17.8 and 20.5 times in MP46 and MM66 respectively. The effect of the single or any combinational treatment on the line OMM1 was minor; the relative caspase activity did not reach 2-fold increase in any case.

Since the combinations containing Trabectedin demonstrated more potent activation of caspases 3 and 7 than the combination of CX-4945 and Foretinib, we narrowed our further study to these two combinations.

In order to clarify the mechanism of action of the selected combinations in more detail, we examined their effect on cell cycle progression of the following UM cell lines: MM66, MP38, MP46, OMM1, and OMM2.5 (Fig. 1G and Supplementary Fig. 1F-I). The cells treated

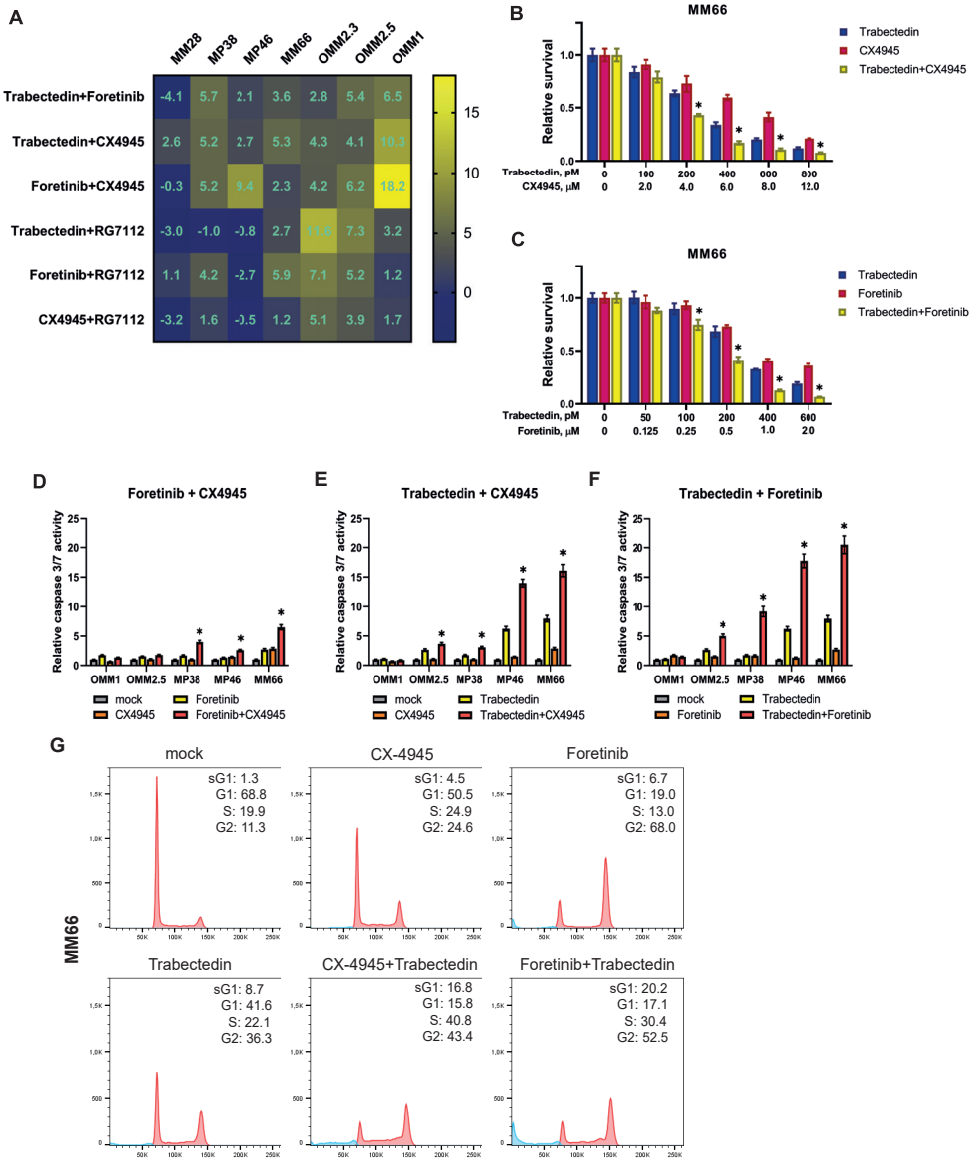

Figure 1. Trabectedin synergizes with CX-4945 and with Foretinib in growth inhibition and apoptosis induction in UM cell lines. **(A)** The matrix of the highest Excess over Bliss (EoB) synergy scores of each treatment per cell line. **(B-C)** Effect of Trabectedin (blue bars), CX-4945 **(B)** or Foretinib **(C)** (magenta) and their combination (yellow) on MM66 cell viability after 5 days of treatment. Significant ($p<0.05$) reduction of viability in combinational treatment comparing to both of the single treatments is indicated with (*), statistical analysis was performed using one-way ANOVA, error bars present mean ± SEM, n=3. **(D-F)** Induction of apoptosis in UM cell lines by the most synergistic combinations. Activity of caspases 3/7 was measured after 5 days of treatment; significant ($p<0.05$) elevation of caspases 3/7 activity in combinational treatment comparing to both of the single treatments is indicated with (*), statistical analysis was performed using one-way ANOVA, error bars present mean ± SEM, n=3. The concentrations of the compounds are listed in Suppl. Table 2. **(G)** Effect of Trabectedin alone or in combination with either CX-4945 or Foretinib on cell cycle progression of MM66 after 3 days of treatment. At least 3 independent replicates were performed,a representative experiment is shown; the concentrations of compounds are listed in Suppl. Table 5.

with Foretinib alone were arrested in G2 phase. Monotreatment with CX-4945 also lead to accumulation of the cells in a G2 phase, but to lesser extent than by Foretinib. The cells treated with Trabectedin alone accumulated in S and G2 phases. The number of the subG1 cells, indicating cell death, increased significantly upon treatment with Trabectedin but less with CX-4945 or Foretinib. These effects were substantial in MM66, MP38, MP46, but less pronounced in OMM1 and OMM2.5.

The cells treated with the combination of Trabectedin with either Foretinib or CX-4945 were arrested in G2 phase. The number of the cells in subG1 fraction rose drastically compared to single treatment in cell lines MM66, MP46, MP38, but the effect on OMM1 was less pronounced, what correlated to the aforementioned induction of caspase 3/7 activity. The significant increase of the subG1 confirms the synergism of the combinations and the induction of cell death upon the treatments.

Induction of apoptosis is regulated by several factors, among which the balance between the expression of Bcl-2 family members, and therefore we evaluated the expression of several of these genes after 24 hours of the treatment. In general, the expression of anti-apoptotic gene *Bcl-2* decreased and the expression of pro-apoptotic genes *Bim*, *Bmf* increased after the treatment with the combination Trabectedin-CX-4945 (Fig. 2A). The effect of the combination Trabectedin-Foretinib on the expression of the tested genes was less explicit and it varied per cell line (Fig. 2B). Expression of other Bcl-2 family members were either not affected or changed only in a subset of the tested cell lines.

Verification of the target engagement of the selected compounds

CX-4945 targets Casein Kinase 2 and affects splicing

To verify the target engagement of the selected compounds, we performed immunoblots and mRNA analyses in a subset of the cell lines, which represents both *GNA11* and *GNAQ* mutations and BAP1-positive or negative status. The concentrations of the compounds corresponded to 50 percent growth inhibition after 5 days.

The treatment with CX-4945 reduced the phosphorylation of AKT on Serine 129, the reported Casein Kinase 2 phosphorylation site [49] (Fig. 2C). Additionally, CX-4945 has been shown to affect Cdc2-like kinases (Clk's), which are essential for the regulatory phosphorylation of SRSF proteins involved in splicing control [50]. To examine this effect in UM, we analysed the splicing of the *Ell* mRNA and *Mdmx* mRNA [51]. Effects on *Ell* splicing were found in three tested cell lines, the most pronounced in MM66 cells after 8 hours treatment (Fig. 2D). Moreover, CX-4945 changed the balance between *Mdmx-FL* and *Mdmx-S* mRNA; again, the effect was strongest in MM66 cells and after 8 hours of treatment.

Trabectedin induces DNA-damage response

Trabectedin interacts with the “minor groove” of DNA, activating DNA damage response cascade, among its many biological effects. The downstream targets of Trabectedin were investigated in the experiments with its combinations in 4 cell lines, MP38, MP46, MM66 and OMM1 treated for 24 hours. The results of protein analyses upon treatment with Trabectedin, CX-4945 or the combination are presented in Fig. 2E and Suppl. Fig. 2A. The treatment with Trabectedin resulted in the phosphorylation and stabilization of p53 as a consequence of the DNA damage, in agreement with the previous report [52, 53]. Elevation of *Mdm2* and *CDKN1A*

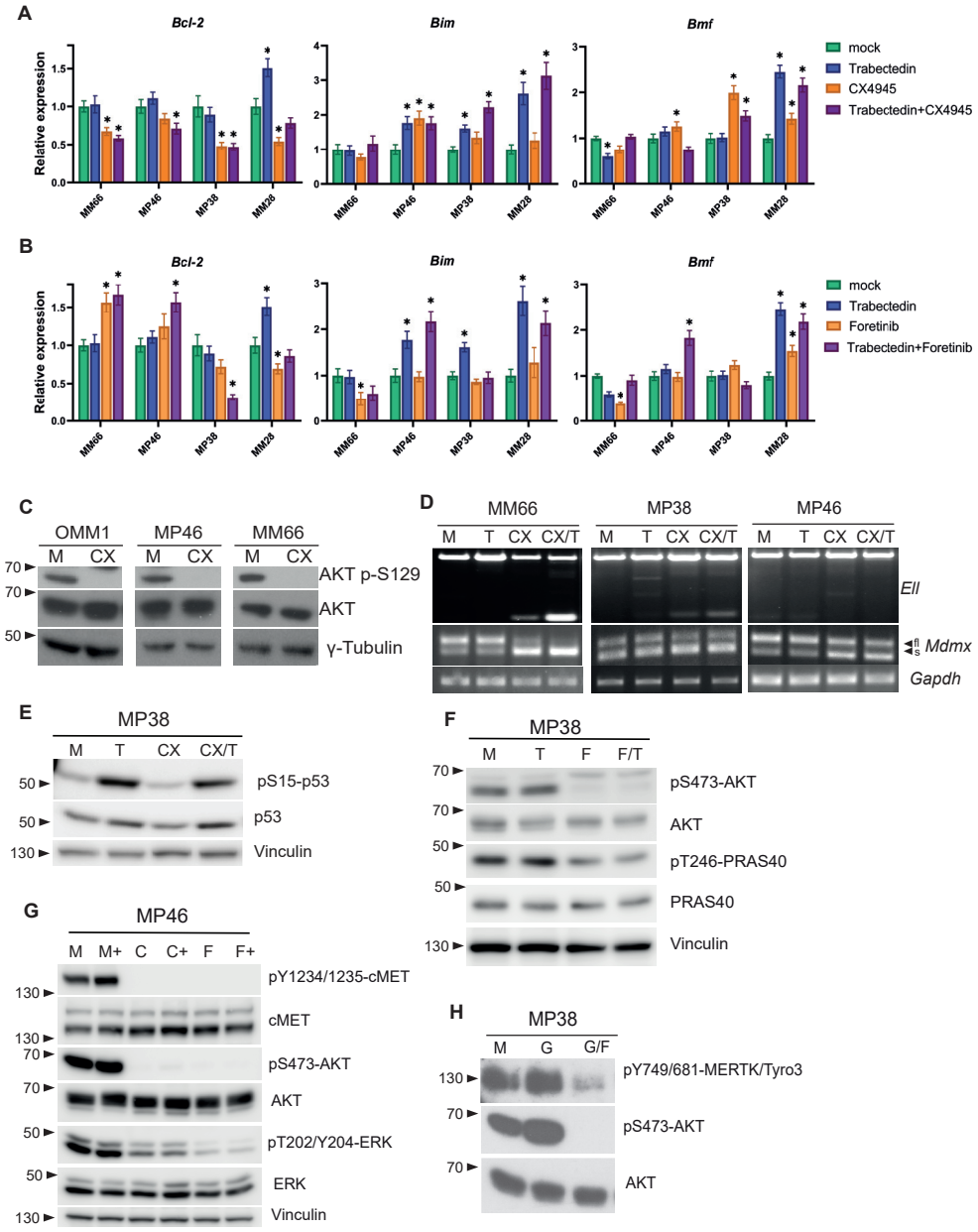

Figure 2. Molecular effects of Trabectedin, CX-4945 and Foretinib. **(A-B)** Expression of *Bcl-2*, *Bim* and *Bmf* mRNA upon 24h treatments with Trabectedin in combination with CX-4945 **(A)** or Foretinib **(B)** in UM cell lines. Significant ($p<0.05$) change in mRNA expression compared to the control is indicated with (*), statistical analysis was performed using one-way ANOVA, error bars present mean ± SEM, n=3. The concentrations of the compounds for this and the following experiments are listed in Suppl. Table 3, if not specified. **(C)** The effect of treatment with CX-4945 (CX) for 24h on phosphorylation of AKT on S129, a reported Casein Kinase 2 phosphorylation site. γ-Tubulin expression was used as a loading control. **(D)** The effect of Trabectedin (T), CX-4945 (CX) or the combination (CX/T) treatment for 8h on splicing of the *Ell* and *Mdmx* mRNA. *Gapdh* mRNA expression was used as a control.

< Figure 2. (continued) **(E-F)** MP38 cells were either not treated (M) or treated with Trabectedin (T), CX-4945 (CX) or the combination (CX/T) **(E)** or Foretinib (F) or the combination (F/T) **(F)** for 24h, after which cells were harvested and expression of the indicated proteins was analysed; Vinculin was used as a loading control. **(G)** MP46 cells were grown on 0.5% FCS for 6 hrs. Subsequently, they were either not pre-treated (M) or pre-treated with either Foretinib (F; 4 μM) or Cabozantinib (C; 4 μM) for two hours after which the cells were either not-stimulated or stimulated with a mixture of HGF and GAS6 (50 and 300 ng/ml, respectively, indicated with +) for 20 minutes, then the cells were harvested for protein lysates. **(H)** MP38 cells, grown in 0.5% serum for 6 hours, were either not pre-treated (M) or pre-treated with Foretinib (F; 4 μM) for 2 hours, after which both untreated and Foretinib pre-treated cells were then stimulated with GAS6 (G; 300 ng/ml) for 20 minutes and collected for analysis. Total AKT was used as a loading control.

mRNA levels could be observed, indicating activation of p53 transcriptional activity (Suppl. Fig. 2B).

Foretinib inhibits activity of c-Met and TAM receptors

Foretinib has been reported to inhibit activity of c-MET, VEGFR2 and the TAM receptors (TYRO3, AXL, MERTK). Activated c-MET, as determined by phosphorylation on tyrosines 1234/1235, is not or hardly detectable in most of UM cell lines: MP46 and MP38 (medium), OMM1, OMM2.3, OMM2.5, MM28 cells (just detectable) (Suppl. Fig. 2C). Expression of AXL could not be detected in any metastatic UM cell line or a primary BAP1-negative cell line, although AXL is expressed in Mel285 and Mel290, primary UM cell lines not carrying *GNAQ/11* mutations. On the contrary, MERTK is highly expressed in the tested cell lines, except for Mel285 and Mel290. TYRO3 is abundantly present in all the tested UM cell lines, what correlates with the observation that expression of *TYRO3* is highest in uveal melanoma among all tumor types analyzed in cBioportal.org database [54, 55].

Inhibition of the RTKs by Foretinib (alone or in combination with Trabectedin) resulted in moderation of AKT signalling, which is illustrated in Fig. 2F and Suppl. Fig. 2D by depletion of phosphorylation of AKT on serine 473, and drop in phosphorylation of its downstream target PRAS40. To show the effect of Foretinib on activated c-MET, we incubated MP46 cells (not pre-treated or pre-treated with either Foretinib or Cabozantinib, another clinically relevant c-MET inhibitor), with a mixture of Growth Arrest Specific 6 (GAS6, the ligand of TAM receptors) and Hepatocyte Growth Factor (HGF, the ligand of c-M ET), which stimulates both c-MET phosphorylation and activation of the TAM receptors. Both Foretinib and Cabozantinib strongly diminished the level of phosphorylated c-MET and reduced the amount of activated AKT and ERK, indicating the efficacy of these compounds (Fig. 2G).

Additionally, we compared the effect of Foretinib and the specific c-MET inhibitor INC280 (Capmatinib) on UM cells, stimulated with HGF. MP38 cells, serum-starved over-night, were pre-incubated with either vehicle, Foretinib or INC280 for two hours. Subsequently, the cells were either treated with vehicle or with HGF, for 20 minutes. The treatment with HGF strongly increased the levels of activated c-MET, activated AKT and activated ERK (Suppl. Fig. 2E). Both Foretinib and INC280 completely abrogated the stimulation of c-MET. However, INC280 only prevented the HGF effect, while Foretinib reduced the levels of activated AKT and ERK beyond basal, low serum levels, suggesting the inhibition of additional targets apart from c-MET.

Moreover, Foretinib and Cabozantinib had effect on UM cell growth, while INC280 did not inhibit proliferation of all the tested cell lines, irrespective of their basal c-MET activity (Suppl. Fig. 2F). Therefore, specific inhibition of c-MET might not be sufficient for blocking the growth of UM metastases.

To investigate the impact of Foretinib on the activity of TAM receptors in UM cells we pre-treated MP38, grown in 0.5% serum for 6 hours, with Foretinib or vehicle for 2 hours, then

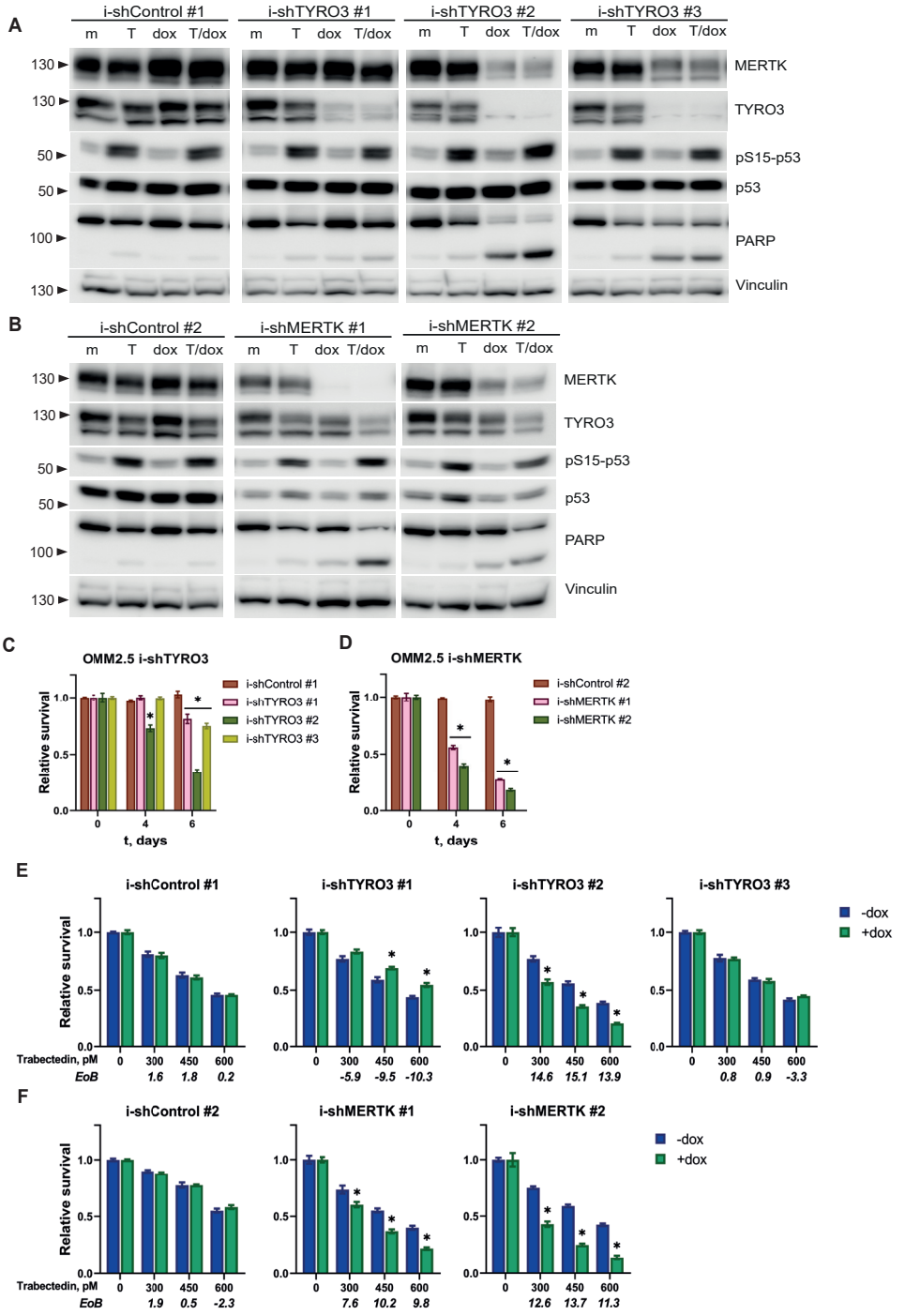
A
i-shControl #1
i-shTYRO3 #1
i-shTYRO3 #2
i-shTYRO3 #3
m T dox T/dox
130
130
50
50
100
130
MERTK
TYRO3
pS15-p53
p53
PARP
Vinculin
B
i-shControl #2
i-shMERTK #1
i-shMERTK #2
MERTK
TYRO3
pS15-p53
p53
PARP
Vinculin
C
OMM2.5 i-shTYRO3
Relative survival
t, days
i-shControl #1
i-shTYRO3 #1
i-shTYRO3 #2
i-shTYRO3 #3
D
OMM2.5 i-shMERTK
i-shControl #2
i-shMERTK #1
i-shMERTK #2
E
i-shControl #1
i-shTYRO3 #1
i-shTYRO3 #2
i-shTYRO3 #3
-dox
+dox
Trabectedin, pM 0 300 450 600
EoB 1.6 1.8 0.2
-5.9 -9.5 -10.3
14.6 15.1 13.9
0.8 0.9 -3.3
F
i-shControl #2
i-shMERTK #1
i-shMERTK #2
1.9 0.5 -2.3
7.6 10.2 9.8
12.6 13.7 11.3

< Figure 3. Effects of genetic depletion of TYRO3 and MERTK in combination with Trabectedin on UM cells.
(A-B) OMM2.5 cells containing i-shControl or i-shTYRO3 vectors **(A)** or i-shMERTK vectors **(B)** were seeded into 6 well-plates. Next day, the cells were treated with either 30 ng/ml doxycycline (dox) or vehicle (m). Two days later all wells were refreshed with medium with or without doxycycline, and with or without 300 pM Trabectedin (T). This treatment was repeated every other day for total duration of 7 days of doxycycline (5 days Trabectedin). **(C-D)** OMM2.5 cells containing i-shControl or i-shTYRO3 vectors **(C)** or i-shMERTK vectors **(D)** were seeded into duplicate 96 well-plates; at the end of the same day when the cells were attached, the medium was supplemented with 30 ng/ml doxycycline (20 ng/ml in case of i-shTYRO3#2). Medium plus or minus doxycycline was refreshed every other day. The plates were analysed after 4 days and duplicate plates after 6 days. Significant reduction ($p<0.05$) of viability comparing to a control (Day 0) is indicated with (*), statistical analysis was performed using one-way ANOVA, error bars present mean ± SEM, n=3. **(E-F)** OMM2.5 cells containing either i-shControl or i-shTYRO3 vectors **(E)** or i-shMERTK vectors **(F)** were seeded into 96 well-plates; at the end of the same day when cells were attached, the medium in half of the wells was supplemented with 30 ng/ml doxycycline (20 ng/ml in case of i-shTYRO3#2). The next day (day 1) Trabectedin was added, at day 2 the treatment with doxycycline and Trabectedin was refreshed and at day 4 the cell viability was assessed. Significant ($p<0.05$) difference in viability of doxycycline-treated samples comparing to vehicle treated samples is indicated with (*), statistical analysis was performed using t-test, error bars present mean ± SEM, n=3.

stimulated the cells with GAS6, an activating ligand for TAM receptors. The results presented in Fig. 2H demonstrate that GAS6 stimulation increased the levels of activated AKT, which was completely abrogated by Foretinib treatment, showing the efficacy of Foretinib against the TAM receptors. The phosphorylation of TYRO3/MERTK was increased by GAS6 and was strongly reduced by Foretinib treatment.

Inhibition of MERTK is important for synergistic combination with Trabectedin

In order to clarify the importance of inhibition of TAM receptors in the combination with Trabectedin, we generated derivatives from UM cell line OMM2.5, containing vectors for either doxycycline-inducible knockdown of *TYRO3* (Fig. 3A) or *MERTK* (Fig. 3B). The protein levels of either MERTK and TYRO3 dropped significantly upon induction of corresponding shRNAs. Moreover, we noticed that the level of MERTK decreased upon induction of shTYRO3 #2 and #3.

The depletion of expression of both proteins led to retardation of cell growth, however, the effect of MERTK knockdown was greater than the depletion of TYRO3. After 4 days of doxycycline induction, expression i-shTYRO3 #2 slowed down the growth of OMM2.5 cells, while the effect of the other i-shTYRO3 appeared only after 6 days of induction (Fig. 3C). Growth retardation of the cells expressing shMERTK was apparent already after 4 days of induction, and only about 25% of the cells left viable two days later (Fig. 3D).

When the knockdown of MERTK was combined with various doses of Trabectedin, we detected additional growth reduction, and the positive values of Excess over Bliss scores indicated synergism (Fig. 3F). The effect of Trabectedin alone on survival was even stronger than the one of the combinations with shTYRO3 #1, indicating not additive and even slight antagonistic action. However, synergism was observed in case of i-shTYRO3 #2 (Fig. 3E). This effect could be present due to simultaneous decline of expression of both TYRO3 and MERTK by shTYRO3 #2. Downregulation of MERTK by this shRNA was most likely indirect, because it took place only after the prolonged treatment with doxycycline, and the sequences targeting *TYRO3* mRNA are very distinct from sequences in *MERTK* mRNA.

The synergistic effect of the combination of MERTK knockdown and Trabectedin was demonstrated also by the analysis of cleaved PARP, a marker of apoptosis (Fig. 3B). The level of cleaved PARP was elevated (and the level of full-length PARP dropped) after treatment with combination of doxycycline and Trabectedin, comparing to the single treatments; the effect

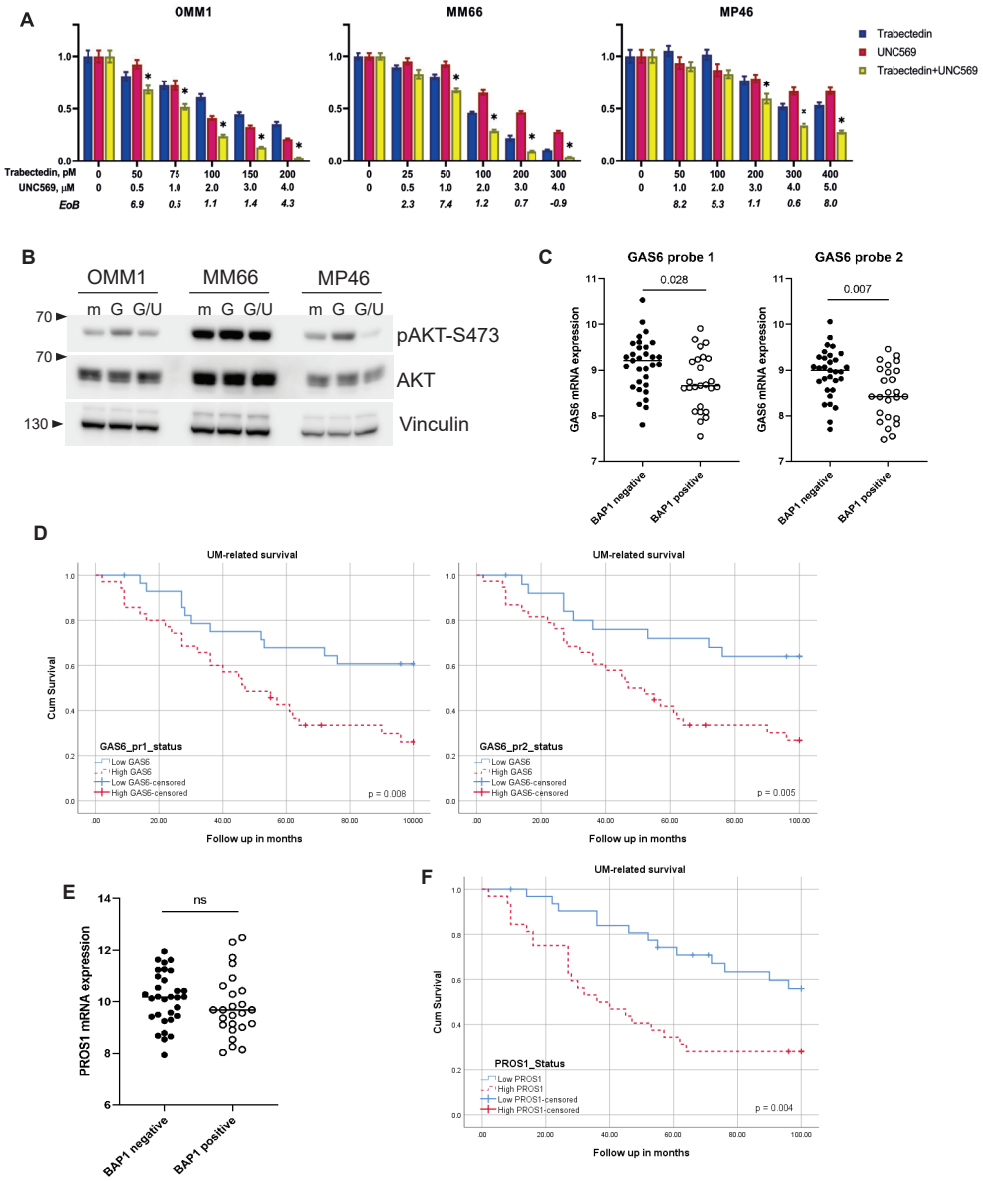

Figure 4. The higher mRNA expression of TAM receptors' ligands *GAS6* and *PROS1* correlates with BAP1-negative status of the tumors and worse prognosis for UM patients. **(A)** The effect of Trabectedin (blue bars), UNC569 (magenta) and their combination (yellow) on viability of OMM1, MM66, MP46 cells after 5 days of treatment. Significant ($p<0.05$) reduction of viability in combinational treatment comparing to both of the single treatments is indicated with (*), statistical analysis was performed using one-way ANOVA, error bars present mean ± SEM, n=3. **(B)** UM cell lines were seeded into 6 well-plates; next day, the medium was supplemented with UNC569 (5 µM). 6 hours later 300 ng/ml GAS6 was added, and 20 min later the samples were harvested for analysis. m-control, G-GAS6-treated samples, G/U- UNC569- and GAS6-treated samples. **(C)** Correlation of *GAS6* mRNA expression with BAP1 status of the tumors in LUMC cohort. Left plot represents probe 1, right plot- probe 2. **(D)** Analysis of the UM-specific survival related to *GAS6* expression in LUMC patient cohort (n=64). GAS6 status split at inflection point, left plot represents probe 1 (n=29 low, n=35 high) right plot- probe 2 (n=26 low, n=38 high). **(E)** Correlation of *PROS1* mRNA expression with BAP1 status of the tumors in LUMC cohort. **(F)** Analysis of the UM-specific survival related to *PROS1* expression in LUMC patient cohort (n=64; split at the median, n=32 high, n=32 low).

was also valid for the shTYRO3 #2, but less pronounced in shTYRO3 #1 and #3 (Fig. 3A).

Confirming the results upon depletion of MERTK, we found that UM cell lines are sensitive in low micromolar range to pharmacological inhibition of MERTK by UNC569, as illustrated in Figure 4A and Suppl. Fig 3A. The combination of UNC569 with Trabectedin synergistically slowed down the growth of UM cell lines, resembling the effects of Trabectedin in MERTK depleted cells. The target engagement of UNC569 is demonstrated in Fig. 4B: UM cell lines OMM1, MM66 and MP46 either not pre-treated or pre-treated with UNC569 were stimulated with the ligand of TAM receptors GAS6. Addition of GAS6 activated AKT signaling thus increased phosphorylation of AKT on Ser473, but pre-treatment with UNC569 completely blocked this upregulation.

Overall, these results indicate importance of inhibition of TAM receptors, especially MERTK, for growth of UM cell lines and synergistic effect of the combination with Trabectedin.

Having demonstrated the effect of MERTK control on proliferation of UM cells, we decided to examine if expression of MERTK or its ligands could be related to metastatic potential of UM and survival of metastatic UM patients. We analyzed mRNA expression of *MERTK*, *GAS6* and *PROS1* in two cohorts of UM patients: LUMC cohort including 64 cases (Figures 4C, F and Suppl. Fig. 3F) and TCGA cohort including 80 cases (Suppl. Fig. 3B, C, H). We stratified the cases by expression of *BAP1*, as loss of BAP1 expression represents a crucial predisposing factor for development of the UM metastases. The mRNA expression of *GAS6* turned out to be significantly elevated in BAP1-negative tumors compared to BAP1-positive tumors in both cohorts (Fig. 4C and Suppl. Fig. 3B). A similar increase of *PROS1* expression was found only in TCGA cohort (Suppl. Fig. 3C), but not in LUMC cohort (Fig. 4F). The mRNA expression of *MERTK* did not differ between BAP1- positive and -negative groups in either cohort (Suppl. Fig. 3F and H).

The mRNA expression of *GAS6* and *PROS1* negatively correlated with survival of UM patients in LUMC cohort, as demonstrated in Fig. 4D and F. However, in TCGA cohort we found the significant effect of *PROS1* expression on survival (Suppl. Fig. 4E), but not of *GAS6* expression (Suppl. Fig. 3D). The mRNA expression of *MERTK* did not affect uveal melanoma related death in any of the cohorts (Suppl. Fig. 3G, I).

The correlation of the expression of the ligands *GAS6* and *PROS1* with *BAP1* status and survival of UM patients highlights the significance of MERTK activity for metastases progression in UM patients.

Cabozantinib mimics the synergistic effects of Foretinib in combination with Trabectedin

The main purpose of our project is to investigate potential therapeutic options for the patients with metastatic UM. Since commercial development of Foretinib has been discontinued during the course of our studies, we decided to substitute Foretinib with Cabozantinib for the experiments *in vivo*. Cabozantinib has been FDA-approved for metastatic differentiated thyroid cancer and currently undergoes clinical studies for advanced tumors of other types [56] including uveal melanoma [57].

We were able to reproduce the results of *in vitro* experiments when Foretinib was replaced by Cabozantinib. UM cell lines were sensitive to Cabozantinib in micromolar concentrations (Suppl. Fig. 2F), the effect on survival was synergistically enhanced in combination with Trabectedin (Fig. 5A and Suppl. Fig. 3A).

The combination Trabectedin-Cabozantinib strongly induced caspase 3/7 activity in the

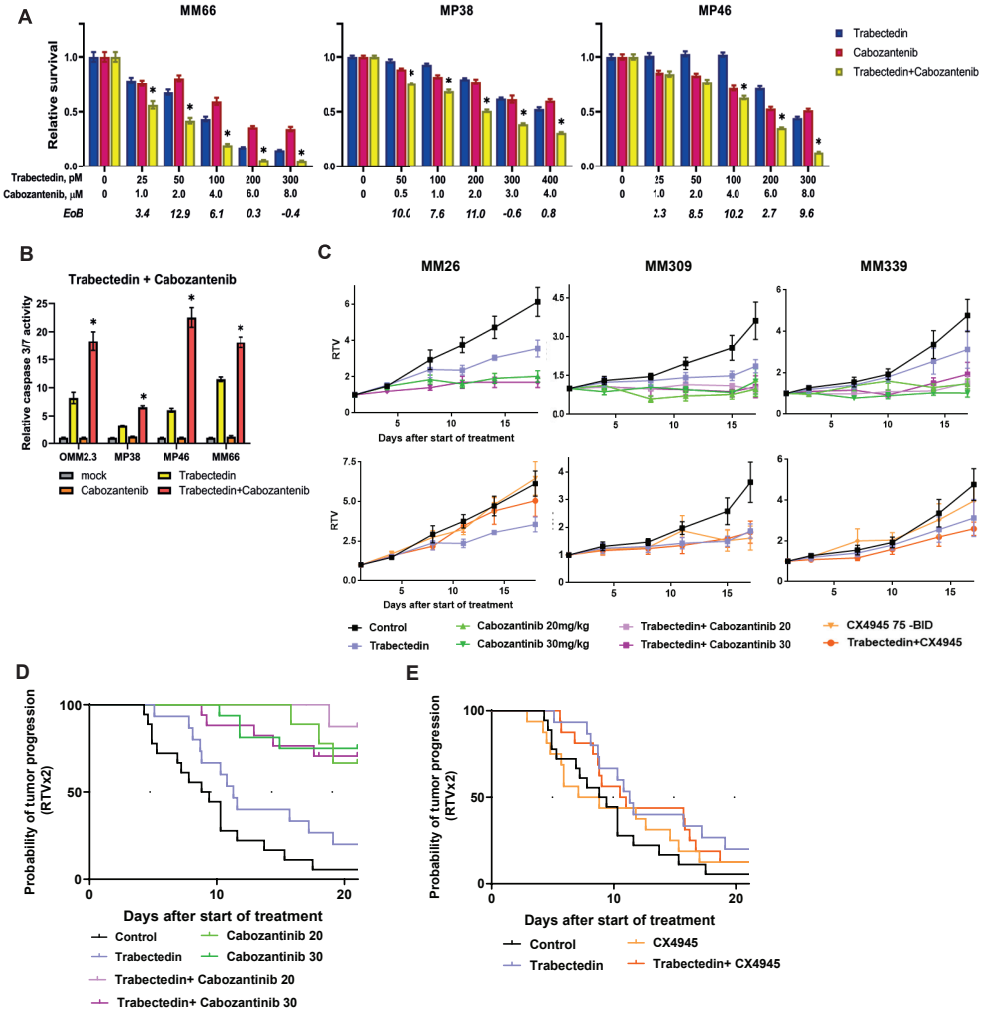

Figure 5. Cabozantinib, similar to Foretinib, is synergistic with Trabectedin *in vitro*, but not *in vivo*. **(A)** The effect of Trabectedin (blue bars), Cabozantinib (magenta) and their combination (yellow) on viability of MM66, MP38 and MP46 cells after 5 days of treatment. Significant ($p<0.05$) reduction of viability in combinational treatment comparing to both of the single treatments is indicated with (*), statistical analysis was performed using one-way ANOVA, error bars present mean ± SEM, n=3. **(B)** Induction of apoptosis in UM cell lines by Trabectedin, Cabozantinib or the combination. Activity of caspases 3/7 was measured after 5 days of treatment, 200 pM of Trabectedin was applied to MM66 and OMM2.3, 400 pM to MP38 and MP46; 4 µM of Cabozantinib was applied to MP38 and MM66, 8 µM to OMM2.3 and MP46. Significant ($p<0.05$) elevation of caspases 3/7 activity in combinational treatment comparing to both of the single treatments is indicated with (*), statistical analysis was performed using one-way ANOVA, error bars present mean ± SEM, n=3. **(C)** Relative tumor volume (RTV) upon treatments with Trabectedin, Cabozantinib, CX-4945 or the combinations. The UM PDXs MM26, MM309 and MM339 were treated either with Trabectedin 0.125 mg/kg, IV, weekly, or with Cabozantinib at 20 or 30mg/kg, daily, 5 days per week, or with CX-4945 at 75 mg/kg, BID, 5 days per week, or with a combination of the drugs. Tumor growth was evaluated by plotting mean RTV ± SEM for each group. For MM26, n= 6 independent PDX (Trabectedin and Trabectedin+ CX-4945); n=7 independent PDX (Control, Cabozantinib, CX-4945); n=8 (Trabectedin+Cabozantinib). For MM309, n=4 for all groups except Control and CX-4945, n=5. For MM339, n=5 for all groups except Control and Trabectedin+Cabozantinib 20mg/kg, n=6. **(D-E)** Probability of progression after Trabectedin treatment with or without Cabozantinib at 20 and 30 mg/kg, daily **(D)** or CX-4945 at 75 mg/kg, BID, daily **(E)**, taking tumor doubling time into account.

tested UM cell lines, as demonstrated in Fig. 5B.

Cabozantinib, as well as Foretinib, efficiently inhibit both c-MET and TAM receptors signaling, what has been demonstrated in Fig. 2G.

The results of the combinations of Trabectedin with CX-4945 and with Cabozantinib were promising in cell culture experiments. Therefore, it was decided to test the efficacy of these combinations on UM PDX models *in vivo*.

In vivo experiments

Three different UM PDXs have been included in our *in vivo* experiments, i.e. MM26, MM309, and MM339. Change in relative tumor volume (RTV) for each treatment is demonstrated in Figure 5C, overall response rate (ORR)- in Suppl. Fig. 4B, and Figure 5D and E represent probability of tumor progression (doubling time) cumulative for all three models.

Looking at efficacy of each tested monotherapy, we observed that Trabectedin alone induced tumor growth inhibition (TGI) of 42% (p=0.0157), 49%, and 35% in MM26, MM309, and MM339 treated PDXs, respectively, with an ORR of 47%. CX-4945 demonstrated a slight antitumor activity in MM26 and MM339 models; the effect was more profound on the MM309 PDX, an ORR represented 27%. Inversely, Cabozantinib blocked tumor growth in all treated PDXs in both tested dosages, with an ORR of 100 and 93% in the 20 mg/kg/day or 30 mg/kg/day groups, respectively.

We did not observe additive efficacy after combining Trabectedin with CX-4945 administration. Similarly, we did not observe additive effect after administration of Trabectedin in combination with Cabozantinib, irrespectively of Cabozantinib dosage.

Discussion

In recent years various therapeutics have been developed and tested in the clinic in order to improve the outcome for the patients with metastatic uveal melanoma [8].

DNA-damaging chemotherapeutics, mainly alkylating agents, have been widely investigated as potential therapy for metastatic UM, but so far, they have demonstrated limited effect on overall survival [58-61]. Trabectedin is a DNA-damaging agent with a distinct, complex mechanism of action. It binds to DNA minor grove, forms adducts and bends DNA, causing DNA damage response; it interacts with proteins bound to DNA, like Rad13, and affects DNA repair and transcription [62]. In addition, Trabectedin affects the tumor microenvironment and activates immune response [63]. Trabectedin has been FDA approved as the second line therapy for metastatic soft tissue sarcoma and has been tested in the clinic for treatment of various types of solid tumors [64, 65].

In this study we showed that Trabectedin inhibits proliferation and induces apoptosis in UM cell lines, and combining Trabectedin with the CK2/Clk-inhibitor CX-4945 reduces survival even further. CK2 phosphorylates a wide set of substrates and inhibition of this kinase leads to alterations in multiple metabolic pathways [66, 67]. Since also Trabectedin has multiple targets, it is not possible to pinpoint the key targets underlying the synergistic effect of these compounds. CX-4945 has previously been shown to enhance the effect of -other- DNA-targeting chemotherapeutics, e.g. Cisplatin, Carboplatin, Gemcitabine, Temozolomide and Doxorubicin [68], in the context of various solid tumors and hematological cancers. These promising pre-clinical results have instigated a clinical trial for treatment of cholangiocarcinoma with the combination of CX-4945 with Cisplatin and Gemcitabine [68].

Additionally to CK2, CX-4945 inhibits the activity of the cyclin-like kinases, which are indirectly involved in splicing; however the importance of the latter function of CX-4945 for its anti-proliferative effect is unknown. We found that CX-4945 affects splicing of *Mdmx* mRNA. Targeting MDMX has been previously suggested as a therapeutic option for cells expressing wild-type p53 [51]. The splicing machinery is often affected in UM, as 15% of the tumors carry mutation in splicing factor SF3B1 [33, 69].

Trabectedin significantly inhibited UM PDX tumor growth in mouse models. However, CX-4945 did not significantly affect the tumor growth *in vivo*, and it did not enhance the effect of Trabectedin. Multiple explanations are possible, for example that CX-4945 could not sufficiently penetrate the solid, subcutaneous tumors formed by the PDX models. In conclusion, the *in vitro* promising combinatory treatment with Trabectedin and CX-4945 cannot be confirmed in the *in vivo* PDX models, making it not a promising treatment for metastatic UM patients. The other combination we identified is Trabectedin with the c-MET and TAM receptors inhibitor Foretinib. This combination also synergistically inhibited UM cell proliferation and induced apoptosis. The c-MET inhibitors have been previously investigated as putative therapeutics for metastatic UM [70]. The ligand of c-MET, HGF, is abundantly present in the liver- the most common site of UM metastatic lesions- stimulating activation of the receptor [34, 71]. According to our data, specific inhibition of c-MET activity with the selective inhibitor INC280 does not affect UM cell proliferation *in vitro*, although it does not exclude an effect of c-MET inhibition on the growth of UM metastases in patients. The treatment with Foretinib does inhibit the growth of UM cells, since it affects other targets besides c-MET, e.g. signal transduction of receptor tyrosine kinases MERTK and TYRO3, which are highly expressed in UM. Blocking of MERTK, rather than TYRO3 activity synergizes with Trabectedin, as follows from our experiments with genetic depletion of these receptors. Similarly, MERTK has been considered as the main target of Foretinib in glioblastoma, and the combination of Foretinib with DNA-damaging chemotherapeutic agent Temozolomide has been reported to inhibit the cell proliferation more efficiently than the single treatments [72]. The level of MERTK has been demonstrated to increase after the treatment with several alkylating agents [73], indicating a possible resistance mechanism, and the depletion of MERTK with shRNA enhanced the cytotoxic effect of Temozolomide and Carboplatin [74]. Since during the course of our studies it was found that the development of Foretinib and its clinical use was discontinued, we compared it with the clinically relevant RTK inhibitor Cabozantinib, essentially inhibiting the same receptor tyrosine kinases. Because the *in vitro* results were very promising, the combination of Trabectedin with Cabozantinib was used in the *in vivo* experiments.

As mentioned before, we observed substantial antitumor effect of Trabectedin with an overall-response-rate of 47%, and monotreatment by Cabozantinib essentially completely blocked the further growth of the tumors with an overall response rate of almost 100%. However, Trabectedin could not enhance the effect of monotreatment by Cabozantinib. This finding was somewhat disappointing, but it could be explained by the strong effect of the Cabozantinib treatment, and the fact that Trabectedin can only be administered once a week due to its toxicity profile. Possibly, if Cabozantinib by itself almost fully blocks cell proliferation, Trabectedin cannot have sufficient effect anymore. Also *in vitro*, in most cell lines, the highest concentration of Cabozantinib shows no or very limited synergism with Trabectedin. Therefore, we still believe that the combination of Trabectedin with Cabozantinib or, even better, a more specific MERTK inhibitor is a therapeutic option for metastatic UM patients, also because in these immunocompromised mouse models the effect of Trabectedin on

immuno-microenvironment is not taken into account. In this respect it is interesting to note that more specific MERTK or MERTK/AXL double inhibitors are being tested in clinical trials [75]. Importantly, MERTK has not only cell-intrinsic proliferative and survival functions, but also creates an immunosuppressive environment, inhibition of which might sensitize metastatic UM for immunotherapy. In line with that, the recent findings suggest a mechanistic link between genetic aberrations in UM and activity of MERTK in tumor associated macrophages. According to Kaler et al. [76], BAP1 loss results in up-regulation of a ligand and agonist of MERTK PROS1 in UM cells through epigenetic mechanisms. In turn, membrane bound PROS1 on tumor cells interacts with MERTK on nearby macrophages, leading to phosphorylation of MERTK and activation of downstream signaling that promotes M2 polarization. PROS1 shares structural and functional similarities with GAS6 [77, 78]. According to our analysis of the clinical datasets, *GAS6* expression is, similar to *PROS1*, correlated to BAP1 expression, and it might have the same effects on the tumor microenvironment.

Therefore, we would be very interested to see a clinical trial for UM metastatic patients with the combination of Trabectedin with currently tested MERTK/AXL inhibitor(s).

Acknowledgements

We thank Marco Herold for the gift of the lentiviral vectors to make inducible shRNA expression vectors. We thank Emilie Vinolo for managing UM CURE project. We thank the animal platform of the Institut Curie.

Methods

Cell culture and lentiviral transductions

Cell lines OMM2.5 (RRID:CVCL_C307), OMM2.3 (RRID:CVCL_C306), Mel285 (RRID:CVCL_C303) and Mel290 (RRID:CVCL_C304) (all a gift of Bruce Ksander) and OMM1 (RRID:CVCL_6939)40 were cultured in a mixture of RPMI and DMEM-F12 (1:1) supplemented with 10% FBS and antibiotics. MM28 (RRID:CVCL_4D15), MP38 (RRID:CVCL_4D11), MP46 (RRID:CVCL_4D13), MM66 (RRID:CVCL_4D17) 41 were cultured in IMDM supplemented with 20% FBS and antibiotics. The cell lines were maintained in humidified incubator at 37°C with 5% CO2.

Inducible shRNA knockdown lentiviral vectors were constructed as described previously [42, 43]. Production of lentivirus stocks by transfections into 293T (CVCL_0063) cells essentially as described, but calcium phosphate was replaced with polyethylenimine [44]. Virus was quantitated by antigen capture enzyme-linked immunosorbent assay (ELISA) measuring HIV p24 levels (ZeptoMetrix Corp., New York, NY, USA). Cells were transduced using a multiplicity of infection of 2 in medium containing 8 μg/ml polybrene. Target shRNA sequences to deplete MERTK or TYRO3 and the control sequences are shown in Suppl. Table 1.

Compound screen

Cells were seeded in appropriate concentration in 6 by 6 wells into 96-well plates. The next day the media was supplemented with serial dilutions of a single agent or a combination of two inhibitors. Six concentrations of each inhibitor were used. Viability was assayed after 5 days of treatment using CellTiter-Blue cell viability assay (Promega, Madison, WI, USA). In

each experiment technical triplicates were assessed, and all analyses were performed on three biological replicates.

A putative synergistic effect was calculated using Excess over Bliss algorithm [45, 46].

Foretinib, CX-4945, Cabozantinib, INC280 (Capmatinib) and RG7112 were obtained from Selleck Chemicals (Houston, TX, USA). Trabectedin was a gift from Pharma Mar S.A. (Madrid, Spain).

Caspase 3/7 activity

The cells were seeded in triplicate into white-walled 96-well plates with clear bottom and in clear 96-well plates. The next day the media was supplemented with the single agents and the combination of two inhibitors; the concentrations are listed in Suppl. Table 2. Five days later the caspase 3/7 activity was assessed with the use of the Caspase-Glo 3/7 Assay (Promega) and the cell viability was assessed with the CellTiter-Blue assay (Promega). The caspase activity relative to viability was calculated.

Western blot

The cells were seeded into 6-well plates. The next day the media was supplemented with a single drug or a combination of two agents; the concentrations are listed in Suppl. Table 3. After the treatments the cells were rinsed twice with ice-cold PBS and scraped and lysed with Giordano buffer (50 mM Tris-HCl pH=7.4, 250 mM NaCl, 0.1% Triton X-100, 5 mM EDTA, supplemented with phosphatase- and protease inhibitors. Equal protein amounts were separated on SDS-PAGE and blotted on PVDF membranes (Millipore, Darmstadt, Germany). The membranes were blocked with 10% non-fat dry milk in TBST (10 mM Tris-HCl pH=8.0, 150 mM NaCl, 0.2% Tween-20) and incubated with the primary antibody diluted in 5% BSA/TBST overnight at 4˚C. The membranes were washed with TBST and incubated with HRP-conjugated secondary antibodies (Jackson Laboratories, Bar Harbor, ME, USA). The chemiluminescent signal was visualized using X-ray film or a Chemidoc machine (Bio-Rad, Hercules, CA, USA). The analysis of the blots was performed using Image Lab software (Bio-Rad, Hercules, CA, USA). The primary antibodies are listed in Suppl. Table 4.

Flow cytometry

The cells were seeded into 6-well plates. The next day the media was supplemented with a single drug or a dual combination; the applied concentrations are listed in Suppl. Table 5. After 5 days the cells (including floating cells) were collected with trypsinization, washed two times with ice-cold PBS and fixed with 70% ethanol overnight at 4˚C. The cells were washed with PBS containing 2% FBS, suspended in PBS containing 2% FBS, 50 µg/ml Propidium Iodide, 50 µg/ml RNAse A and incubated 30 min at 37˚C. Flow cytometry was performed using the BD LSR II system (BD Biosciences, Franklin Lakes, NJ, USA). In total 10,000 events were recorded. The data was analyzed using FlowJo v10.6.1 software. The sum of G1, S and G2 percentage was set to 100. The subG1 population was determined as a percentage of the whole population.

RNA isolation and qPCR

The cells were seeded into 6-well plates. The next day media was supplemented with a

single drug or a combination; the concentrations are listed in Suppl. Table 2. After the treatment the cells were collected by scraping in lysis buffer and RNA was isolated using SV Total RNA Isolation System (Promega) according to the manufacturers' protocol. The reverse transcription reaction was performed using ImProm II reverse transcriptase (Promega). qPCR was performed using SYBR green mix (Roche, Basel, Switzerland) in a C1000 Touch Thermal Cycler (Bio-Rad). Relative expression of the tested genes was calculated compared to expression of housekeeping CAPNS1 and SRPR. The primer sequences are listed in Suppl. Table 6.

Analysis of effects of CX-4945 on mRNA splicing was performed with the primers listed in Suppl. Table 7.

In vivo experiments

UM PDX models

Three UM PDX models, MM26, MM309 and MM339 obtained from liver metastatic of human uveal melanoma were used. MM26 is mutated for *GNAQ* and *SF3B1*. MM309 is mutated for *GNAQ* and MM339 for *GNA11*; both are mutated for *BAP1*.

Reagents

Trabectedin was kindly provided by PharmaMar and administered intravenously, weekly. Cabozantinib and CX-4945 were purchased from MedchemExpress. Cabozantinib was formulated in vehicle 3% DMSO, 30% PEG300 and 67% HPCD 20%, and CX-4945 in 10% DMSO, 40% PEG300, 30% polypropylene glycol and 20% H2O. Cabozantinib was administered at 20 and 30 mg/kg, daily, and CX-4945 at 75 mg/kg, BID, daily. Both were administered orally 5 days per week.

In vivo efficacy studies

For efficacy assessments, tumor fragments were transplanted into female SCID mice from Janvier Laboratories. Xenografts were randomly assigned to the different treatment groups when tumors reached a volume comprised between 60 and 260 mm3. Tumor size was measured with a manual caliper twice per week. Tumor volumes were calculated as $V = a \times b2/2$, a being the largest diameter, b the smallest. Tumor volumes were then reported to the initial volume as relative tumor volume (RTV). Means (and SEM) of RTV in the same treatment group were calculated, and growth curves were established as a function of time. Antitumor activity was evaluated by determining tumor growth inhibition (TGI) as follows: percent GI = 100 − (RTVt / RTVc × 100), where RTVt is the mean RTV of treated mice and RTVc is the mean RTV of controls, both for the time point at which antitumor effect was optimal. A meaningful biological effect was defined as a TGI of at least 50%. The statistical significance of the differences observed between the individual RTVs corresponding to the treated and control mice was determined in two-tailed Mann-Whitney tests. Moreover, the response of treatments in all models were evaluated as a function of individual mouse variability, by considering each mouse as a single tumor-bearing entity. Hence, in all *in vivo* experiments, a relative tumor volume variation (RTVV) was calculated for each treated mouse as follows: (RTVt/mRTVc), where RTVt is the relative tumor volume of the treated mouse and mRTVc is the median relative tumor volume of the corresponding control group of corresponding day of treatment. We then calculated (RTVV)-1

for each treated mouse. A tumor was considered to be responding to treatment if (RTVV)-1 was below -0.5. Finally, to assess the impact of treatments on the tumor progression, we evaluated the probability of progression (doubling time) as described [47].

This study was performed in accordance with the recommendations of the European Community (2010/63/UE) for the care and use of laboratory animals. Experimental procedures were approved by the ethics committee of Institut Curie CEEA-IC #118 (Authorization APAFIS# #25870-2020060410487032-v1 given by National Authority) in compliance with the international guidelines.

Clinical data analysis

The LUMC cohort includes clinical, histopathological, and genetic information on 64 UM cases enucleated between 1999 and 2008 at the Leiden University Medical Centre (LUMC). Clinical information was collected from the Integral Cancer Center West patient records and updated in 2021. For each sample, part of the tumor was snap frozen with 2-methyl butane and used for mRNA and DNA isolation, while the remainder was embedded in paraffin after 48 hours of fixation in 4% neutral-buffered formalin and was sent for histological analysis. RNA was isolated with the RNeasy mini kit (Qiagen, Venlo, The Netherlands) and mRNA expression was determined with the HT-12 v4 chip (Illumina, San Diego, CA, USA). BAP1 status (positive or negative) was determined by immunohistochemistry.

TCGA cohort represents 80 primary UM cases enucleated in 6 different centers48. mRNA expression was determined by RNA-seq. BAP1 status (high or low expression) was determined by splitting mRNA expression along the median expression value.

Statistical analyses of the LUMC and TCGA cohorts were carried out in SPSS, version 25 (IBM Corp). For survival analysis, Kaplan-Meier and log-rank test were performed with death due to metastases as endpoint. Cases that died of another or unknown cause were censored. The two subpopulations that were compared in each analysis were determined by splitting the total cohort along the median value of mRNA expression for each analyzed gene.

The study was approved by the Biobank Committee of the Leiden University Medical Center (LUMC; 19.062.CBO/ uveamalanoomlab-2019-3; B20.023). The tenets of Declaration of Helsinki were followed.

References

1. Virgili G, Gatta G, Ciccolallo L, et al. Incidence of uveal melanoma in Europe. Ophthalmology. 2007; 114(12): 2309-2315

2. Koutsandrea C, Moschos MM, Dimissianos M, et al. Metastasis rates and sites after treatment for choroidal melanoma by proton beam irradiation or by enucleation. Clin Ophthalmol. 2008; 2(4): 989-995

3. Diener-West M, Reynolds SM, Agugliaro DJ, et al. Screening for metastasis from choroidal melanoma: the Collaborative Ocular Melanoma Study Group Report 23. J Clin Oncol. 2004; 22(12): 2438-2444

4. Alexander HR, Libutti SK, Pingpank JF, et al. Hyperthermic isolated hepatic perfusion using melphalan for patients with ocular melanoma metastatic to liver. Clin Cancer Res. 2003; 9(17): 6343-6349

5. Noter SL, Rothbarth J, Pijl MEJ, et al. Isolated hepatic perfusion with high-dose melphalan for the treatment of uveal melanoma metastases confined to the liver. Melanoma Res. 2004; 14(1): 67-72

6. Meijer TS, Burgmans MC, de Leede EM, et al. Percutaneous Hepatic Perfusion with Melphalan in Patients with Unresectable Ocular Melanoma Metastases Confined to the Liver: A Prospective Phase II Study. Ann Surg Oncol. 2021; 28(2): 1130-1141

7. Dewald CLA, Warnke MM, Bruening R, et al. Percutaneous Hepatic Perfusion (PHP) with Melphalan in Liver-Dominant Metastatic Uveal Melanoma: The German Experience. Cancers. 2022; 14(1): 118

8. Yang J, Manson DK, Marr BP and Carvajal RD. Treatment of uveal melanoma: where are we now? Alternate Journal. 2018; 10, doi: 10.1177/1758834018757175

9. Carvajal RD, Piperno-Neumann S, Kapiteijn E, et al. Selumetinib in Combination With Dacarbazine in Patients With Metastatic Uveal Melanoma: A Phase III, Multicenter, Randomized Trial (SUMIT). J Clin Oncol. 2018; 36(12): 1232-1239

10. Spagnolo F, Grosso M, Picasso V, et al. Treatment of metastatic uveal melanoma with intravenous fotemustine. Melanoma Res. 2013; 23(3): 196-198

11. Falchook GS, Lewis KD, Infante JR, et al. Activity of the oral MEK inhibitor trametinib in patients with advanced melanoma: a phase 1 dose-escalation trial. Lancet Oncol. 2012; 13(8): 782-789

12. Penel N, Delcambre C, Durando X, et al. O-Mel-Inib: A Cancero-pole Nord-Ouest multicenter phase II trial of high-dose imatinib mesylate in metastatic uveal melanoma. Invest New Drug. 2008; 26(6): 561-565

13. Shah S, Luke JJ, Jacene HA, et al. Results from phase II trial of HSP90 inhibitor, STA-9090 (ganetespib), in metastatic uveal melanoma. Melanoma Res. 2018; 28(6): 605-610

14. Rossi E, Pagliara MM, Orteschi D, et al. Pembrolizumab as first-line treatment for metastatic uveal melanoma. Cancer Immunol Immun. 2019; 68(7): 1179-1185

15. Rodrigues M, Mobuchon L, Houy A, et al. Outlier response to anti-PD1 in uveal melanoma reveals germline MBD4 mutations in hypermutated tumors. Alternate Journal. 2018; 9, doi: 10.1038/s41467-018-04322-5

16. Nathan P, Hassel JC, Rutkowski P, et al. Overall Survival Benefit with Tebentafusp in Metastatic Uveal Melanoma. New Engl J Med. 2021; 385(13): 1196-1206

17. Johansson PA, Brooks K, Newell F, et al. Whole genome landscapes of uveal melanoma show an ultraviolet radiation signature in iris tumours. Alternate Journal. 2020; 11, doi: 10.1038/s41467-020-16276-8

18. Yarchoan M, Hopkins A and Jaffee EM. Tumor Mutational Burden and Response Rate to PD-1 Inhibition. New Engl J Med. 2017; 377(25): 2500-2501

19. Robertson AG, Shih J, Yau C, et al. Integrative Analysis Identifies Four Molecular and Clinical Subsets in Uveal Melanoma. Cancer Cell. 2017; 32(2): 204-220

20. Johansson P, Aoude LG, Wadt K, et al. Deep sequencing of uveal melanoma identifies a recurrent mutation in PLCB4. Oncotarget. 2016; 7(4): 4624-4631

21. Moore AR, Ceraudo E, Sher JJ, et al. Recurrent activating mutations of G-protein-coupled receptor CYSLTR2 in uveal melanoma. Nat Genet. 2016; 48(6): 675-680

22. Chen X, Wu QX, Depeille P, et al. RasGRP3 Mediates MAPK Pathway Activation in GNAQ Mutant Uveal Melanoma. Cancer Cell. 2017; 31(5): 685-696

23. Yu FX, Luo J, Mo JS, et al. Mutant Gq/11 Promote Uveal Melanoma Tumorigenesis by Activating YAP. Cancer Cell. 2014; 25(6): 822-830

24. Aalto Y, Eriksson L, Seregard S, Larsson O and Knuutila S. Concomitant loss of chromosome 3 and whole arm losses and gains of chromosome 1, 6, or 8 in metastasizing primary uveal melanoma. Invest Ophth Vis Sci. 2001; 42(2): 313-317

25. Sisley K, Rennie IG, Parsons MA, et al. Abnormalities of chromosomes 3 and 8 in posterior uveal melanoma correlate with prognosis. Gene Chromosome Canc. 1997; 19(1): 22-28

26. Damato B, Dopierala JA and Coupland SE. Genotypic Profiling of 452 Choroidal Melanomas with Multiplex Ligation-Dependent Probe Amplification. Clin Cancer Res. 2010; 16(24): 6083-6092

27. Ewens KG, Kanetsky PA, Richards-Yutz J, et al. Genomic Profile of 320 Uveal Melanoma Cases: Chromosome 8p-Loss and Metastatic Outcome. Invest Ophth Vis Sci. 2013; 54(8): 5721-5729

28. Harbour JW, Onken MD, Roberson EDO, et al. Frequent Mutation of BAP1 in Metastasizing Uveal Melanomas. Science. 2010; 330(6009): 1410-1413

29. Martin M, Masshofer L, Temming P, et al. Exome sequencing identifies recurrent somatic mutations in EIF1AX and SF3B1 in uveal melanoma with disomy 3. Nat Genet. 2013; 45(8): 933-U296

30. Onken MD, Makepeace CM, Kaltenbronn KM, et al. Targeting primary and metastatic uveal melanoma with a G

protein inhibitor. Alternate Journal. 2021; 296, doi: 10.1016/j.jbc.2021.100403

31. de Lange J, Teunisse AFAS, Verlaan-de Vries M, et al. High levels of Hdmx promote cell growth in a subset of uveal melanomas. Am J Cancer Res. 2012; 2(5): 492-507

32. Harbour JW, Roberson EDO, Anbunathan H, et al. Recurrent mutations at codon 625 of the splicing factor SF3B1 in uveal melanoma. Nat Genet. 2013; 45(2): 133-135

33. Furney SJ, Pedersen M, Gentien D, et al. SF3B1 Mutations Are Associated with Alternative Splicing in Uveal Melanoma. Cancer Discov. 2013; 3(10): 1122-1129

34. Mallikarjuna K, Pushparaj V, Biswas J and Krishnakumar S. Expression of epidermal growth factor receptor, ezrin, hepatocyte growth factor, and c-Met in uveal melanoma: An immunohistochemical study. Curr Eye Res. 2007; 32(3): 281-290

35. van Ginkel PR, Gee RL, Shearer RL, et al. Expression of the receptor tyrosine kinase Axl promotes ocular melanoma cell survival. Cancer Res. 2004; 64(1): 128-134

36. Monk BJ, Herzog TJ, Wang G, et al. A phase 3 randomized, open-label, multicenter trial for safety and efficacy of combined trabectedin and pegylated liposomal doxorubicin therapy for recurrent ovarian cancer. Gynecol Oncol. 2020; 156(3): 535-544

37. Borad MJ, Bai LY, Chen MH, et al. Silmitasertib (CX-4945) in combination with gemcitabine and cisplatin as first-line treatment for patients with locally advanced or metastatic cholangiocarcinoma: A phase Ib/II study. J Clin Oncol. 2021; 39(3): 312-312

38. Rayson D, Lupichuk S, Potvin K, et al. Canadian Cancer Trials Group IND197: a phase II study of foretinib in patients with estrogen receptor, progesterone receptor, and human epidermal growth factor receptor 2-negative recurrent or metastatic breast cancer. Breast Cancer Res Tr. 2016; 157(1): 109-116

39. Andreeff M, Kelly KR, Yee K, et al. Results of the Phase I Trial of RG7112, a Small-Molecule MDM2 Antagonist in Leukemia. Clin Cancer Res. 2016; 22(4): 868-876

40. Luyten GPM, Naus NC, Mooy CM, et al. Establishment and characterization of primary and metastatic uveal melanoma cell lines. Int J Cancer. 1996; 66(3): 380-387

41. Amirouchene-Angelozzi N, Nemati F, Gentien D, et al. Establishment of novel cell lines recapitulating the genetic landscape of uveal melanoma and preclinical validation of mTOR as a therapeutic target. Mol Oncol. 2014; 8(8): 1508-1520

42. Herold MJ, van den Brandt J, Seibler J and Reichardt HM. Inducible and reversible gene silencing by stable integration of an shRNA-encoding lentivirus in transgenic rats. P Natl Acad Sci USA. 2008; 105(47): 18507-18512

43. Heijkants RC, Nieveen M, 't Hart KC, Teunisse AFAS and Jochemsen AG. Targeting MDMX and PKC delta to improve current uveal melanoma therapeutic strategies. Alternate Journal. 2018; 7, doi: 10.1038/s41389-018-0041-y

44. Carlotti F, Bazuine M, Kekarainen T, et al. Lentiviral vectors efficiently transduce quiescent mature 3T3-L1 adipocytes. Mol Ther. 2004; 9(2): 209-217

45. Bliss CI. Calculation of Microbial Assays. Bacteriol Rev. 1956; 20(4): 243-258

46. Fitzgerald JB, Schoeberl B, Nielsen UB and Sorger PK. Systems biology and combination therapy in the quest for clinical efficacy. Nat Chem Biol. 2006; 2(9): 458-466

47. Gao H, Korn JM, Ferretti S, et al. High-throughput screening using patient-derived tumor xenografts to predict clinical trial drug response. Nat Med. 2015; 21(11): 1318-1325

48. Robertson AG, Shih J, Yau C, et al. Integrative Analysis Identifies Four Molecular and Clinical Subsets in Uveal Melanoma. Cancer Cell. 2017; 32(2): 204-220

49. Di Maira G, Salvi M, Arrigoni G, et al. Protein kinase CK2 phosphorylates and upregulates Akt/PKB. Cell Death Differ. 2005; 12(6): 668-677

50. Kim H, Choi K, Kang H, et al. Identification of a Novel Function of CX-4945 as a Splicing Regulator. Alternate Journal. 2014; 9, doi: 10.1371/journal.pone.0094978

51. Dewaele M, Tabaglio T, Willekens K, et al. Antisense oligonucleotide-mediated MDM4 exon 6 skipping impairs tumor growth. J Clin Invest. 2016; 126(1): 68-84

52. Erba E, Bergamaschi D, Bassano L, et al. Ecteinascidin-743 (ET-743), a natural marine compound, with a unique mechanism of action. Eur J Cancer. 2001; 37(1): 97-105

53. Soares DG, Escargueil AE, Poindessous V, et al. Replication and homologous recombination repair regulate DNA double-strand break formation by the antitumor alkylator ecteinascidin 743. P Natl Acad Sci USA. 2007; 104(32): 13062-13067

54. Gao JJ, Aksoy BA, Dogrusoz U, et al. Integrative Analysis of Complex Cancer Genomics and Clinical Profiles Using the cBioPortal. Alternate Journal. 2013; 6, doi: 10.1126/scisignal.2004088

55. Cerami E, Gao JJ, Dogrusoz U, et al. The cBio Cancer Genomics Portal: An Open Platform for Exploring Multidimensional Cancer Genomics Data. Cancer Discov. 2012; 2(5): 401-404

56. Choueiri TK, Powles T, Burotto M, et al. Nivolumab plus Cabozantinib versus Sunitinib for Advanced Renal-Cell Carcinoma. New Engl J Med. 2021; 384(9): 829-841

57. Luke JJ, Olson DJ, Allred JB, et al. Randomized Phase II Trial and Tumor Mutational Spectrum Analysis from Cabozantinib versus Chemotherapy in Metastatic Uveal Melanoma (Alliance A091201). Clin Cancer Res. 2020; 26(4): 804-811

58. Schmittel A, Scheulen ME, Bechrakis NE, et al. Phase II trial of cisplatin, gemcitabine and treosulfan in patients with metastatic uveal melanoma. Melanoma Res. 2005; 15(3): 205-207

59. Schinzari G, Rossi E, Cassano A, et al. Cisplatin, dacarbazine and vinblastine as first line chemotherapy for liver metastatic uveal melanoma in the era of immunotherapy: a single institution phase II study. Melanoma Res. 2017; 27(6):

591-595
60. O'Neill PA, Butt M, Eswar CV, Gillis P and Marshall E. A prospective single arm phase II study of dacarbazine and treosulfan as first-line therapy in metastatic uveal melanoma. Melanoma Res. 2006; 16(3): 245-248
61. Kivela T, Suciu S, Hansson J, et al. Bleomycin, vincristine, lomustine and dacarbazine (BOLD) in combination with recombinant interferon alpha-2b for metastatic uveal melanoma. Eur J Cancer. 2003; 39(8): 1115-1120
62. D'Incalci M, Badri N, Galmarini CM and Allavena P. Trabectedin, a drug acting on both cancer cells and the tumour microenvironment. Brit J Cancer. 2014; 111(4): 646-650
63. Ratti C, Botti L, Cancila V, et al. Trabectedin Overrides Osteosarcoma Differentiative Block and Reprograms the Tumor Immune Environment Enabling Effective Combination with Immune Checkpoint Inhibitors. Clin Cancer Res. 2017; 23(17): 5149-5161
64. Demetri GD, von Mehren M, Jones RL, et al. Efficacy and Safety of Trabectedin or Dacarbazine for Metastatic Liposarcoma or Leiomyosarcoma After Failure of Conventional Chemotherapy: Results of a Phase III Randomized Multicenter Clinical Trial. J Clin Oncol. 2016; 34(8): 786-793
65. Vidal L, Magem M, Barlow C, et al. Phase I clinical and pharmacokinetic study of trabectedin and carboplatin in patients with advanced solid tumors. Invest New Drug. 2012; 30(2): 616-628
66. Meggio F, Marin O and Pinna LA. Substrate specificity of protein kinase CK2. Cell Mol Biol Res. 1994; 40(5-6): 401-409
67. Meggio F and Pinna LA. One-thousand-and-one substrates of protein kinase CK2? FASEB J. 2003; 17(3): 349-368
68. D'Amore C, Borgo C, Sarno S and Salvi M. Role of CK2 inhibitor CX-4945 in anti-cancer combination therapy - potential clinical relevance. Cell Oncol. 2020; 43(6): 1003-1016
69. Martin M, Masshofer L, Temming P, et al. Exome sequencing identifies recurrent somatic mutations in EIF1AX and SF3B1 in uveal melanoma with disomy 3. 2013; 45(8): 933-936
70. Surriga O, Rajasekhar VK, Ambrosini G, et al. Crizotinib, a c-Met inhibitor, prevents metastasis in a metastatic uveal melanoma model. 2013; 12(12): 2817-2826
71. Gardner FP, Serie DJ, Salomao DR, et al. c-MET expression in primary and liver metastases in uveal melanoma. 2014; 24(6): 617-620
72. Knubel KH, Pernu BM, Sufit A, et al. MerTK inhibition is a novel therapeutic approach for glioblastoma multiforme. Oncotarget. 2014; 5(5): 1338-1351
73. Sufit A, Lee-Sherick AB, DeRyckere D, et al. MERTK Inhibition Induces Polyploidy and Promotes Cell Death and Cellular Senescence in Glioblastoma Multiforme. Alternate Journal. 2016; 11, doi: 10.1371/journal.pone.0165107
74. Keating AK, Kim GK, Jones AE, et al. Inhibition of Mer and Axl Receptor Tyrosine Kinases in Astrocytoma Cells Leads to Increased Apoptosis and Improved Chemosensitivity. Mol Cancer Ther. 2010; 9(5): 1298-1307
75. Huelse JM, Fridlyand DM, Earp S, DeRyckere D and Graham DK. MERTK in cancer therapy: Targeting the receptor tyrosine kinase in tumor cells and the immune system. Alternate Journal. 2020; 213, doi: 10.1016/j.pharmthera.2020.107577
76. Kaler CJ, Dollar JJ, Cruz AM, et al. BAP1 Loss Promotes Suppressive Tumor Immune Microenvironment via Upregulation of PROS1 in Class 2 Uveal Melanomas. Alternate Journal. 2022; 14, doi: 10.3390/cancers14153678
77. Hafizi S and Dahlback B. Gas6 and protein S. Febs J. 2006; 273(23): 5231-5244
78. Laurance S, Lemarie CA and Blostein MD. Growth Arrest-Specific Gene 6 (gas6) and Vascular Hemostasis. Adv Nutr. 2012; 3(2): 196-203

Supplementary figures

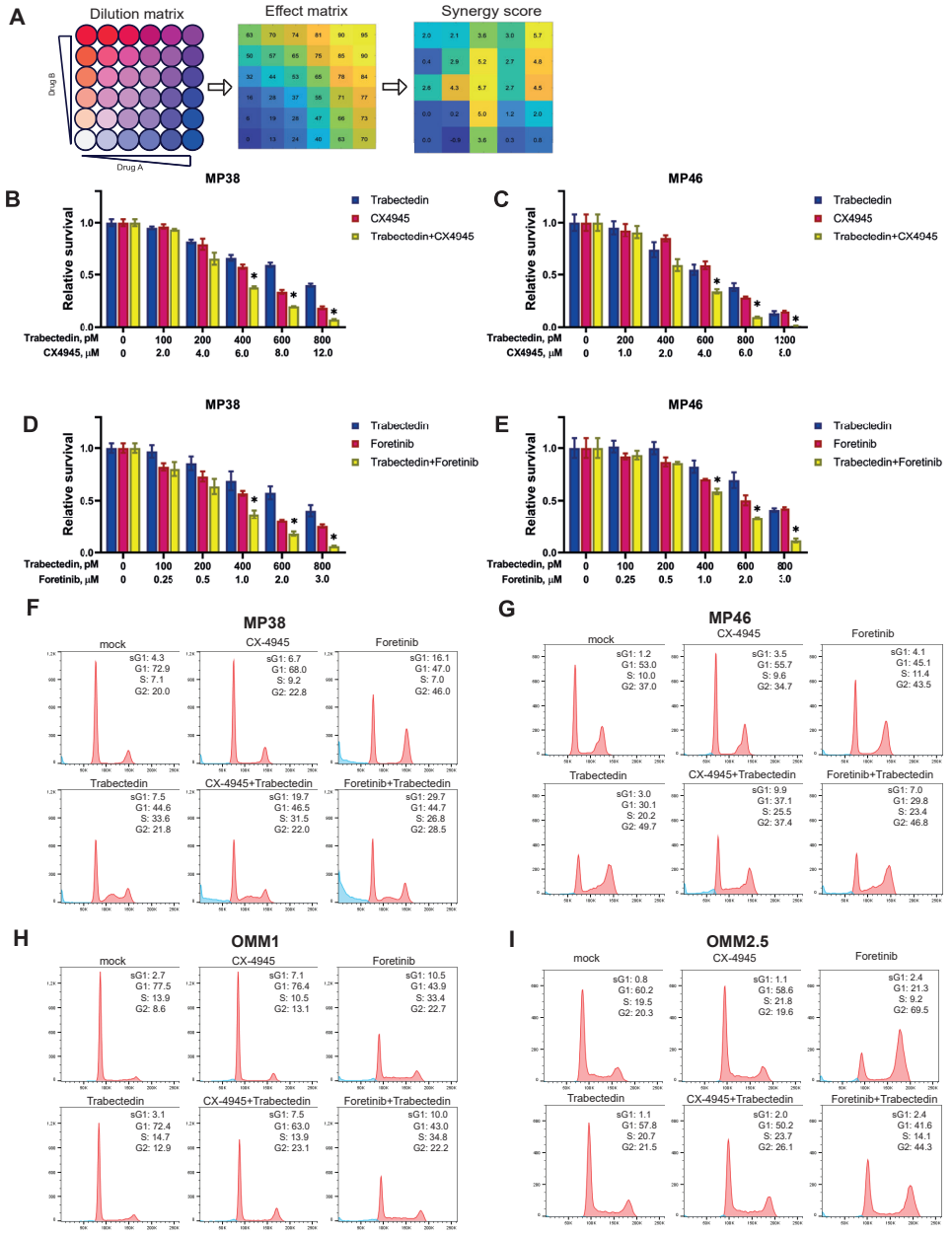

Supplementary figure 1. Workflow of the compound screen and the effect of the selected combinations in UM cell viability. **(A)** Workflow of the compound screen. **(B-C)** Effect of Trabectedin (blue bars), CX-4945 or (magenta) and their combination (yellow) on viability of MP38 **(B)** and MP46 **(C)** cells after 5 days of treatment. **(D-E)** Effect of Trabectedin (blue bars), CX-4945 or (magenta) and their combination (yellow) on viability of MP38 **(D)** and MP46 **(E)** cells after 5 days of treatment. Significant ($p<0.05$) reduction of viability in combinational treatment comparing to both of the single treatments is indicated with (*), statistical analysis was performed using one-way ANOVA, error bars present mean ± SEM, n=3. (F-I) The effect of Trabectedin alone or in combination with either CX-4945 or Foretinib on cell cycle progression of UM cell lines after 3 days of treatment; the concentrations of the applied compounds are listed in Suppl. Table 5.

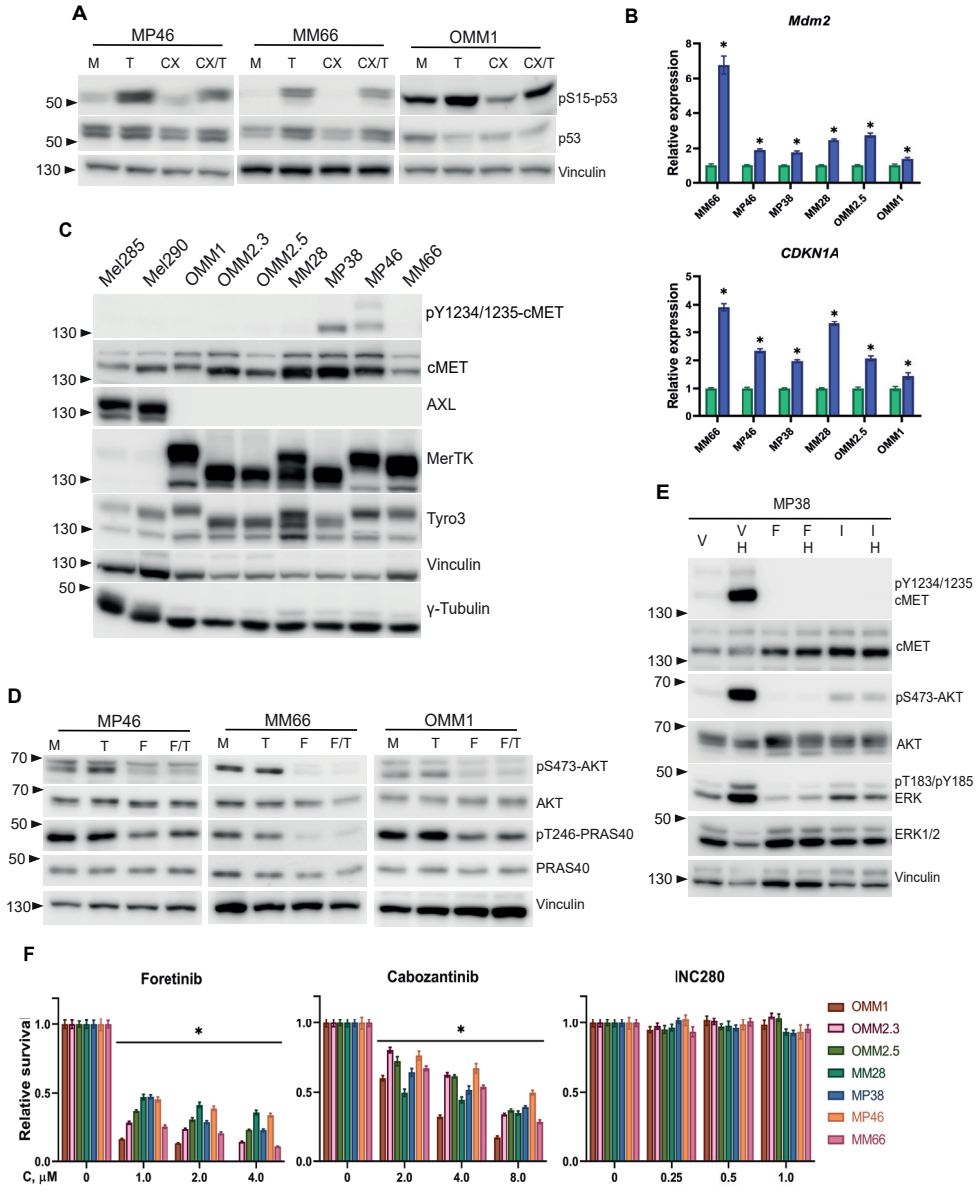

Supplementary figure 2. Verification of target engagement of the selected inhibitors. **(A)** The effect of Trabectedin (T), CX-4945 (CX) or the combination (CX/T) treatment for 24h on p53 signaling. Vinculin was used as a control. **(B)** Expression of *Mdm2* and *CDKN1A* mRNA upon 24h treatments with Trabectedin. Significant ($p<0.05$) change in mRNA expression comparing to the control is indicated with (*), statistical analysis was performed using t-test, error bars present mean ± SEM. **(C)** Expression of c-MET and TAM receptors in UM cell lines. **(D)** The effect of Trabectedin (T), Foretinib (F) or the combination (F/T) treatment for 24h on AKT signaling. Vinculin was used as a control. **(E)** MP38 cells were grown for 16 hours in medium with 0.5% serum, then pre-incubated with either vehicle (M), Foretinib (F; 4 μM) or INC280 (I; 0.1 μM) for 2 hours. Subsequently, the cells were either treated with vehicle or with HGF (H; 50 ng/ml), for 20 minutes after which they were harvested for protein analysis. **(F)** The effect of Foretinib, Cabozantinib and INC280 on UM cell viability after 5 days of treatment. Significant ($p<0.05$) reduction of viability in combinational treatment comparing to the control is indicated with (*), statistical analysis was performed using one-way ANOVA, error bars present mean ± SEM.

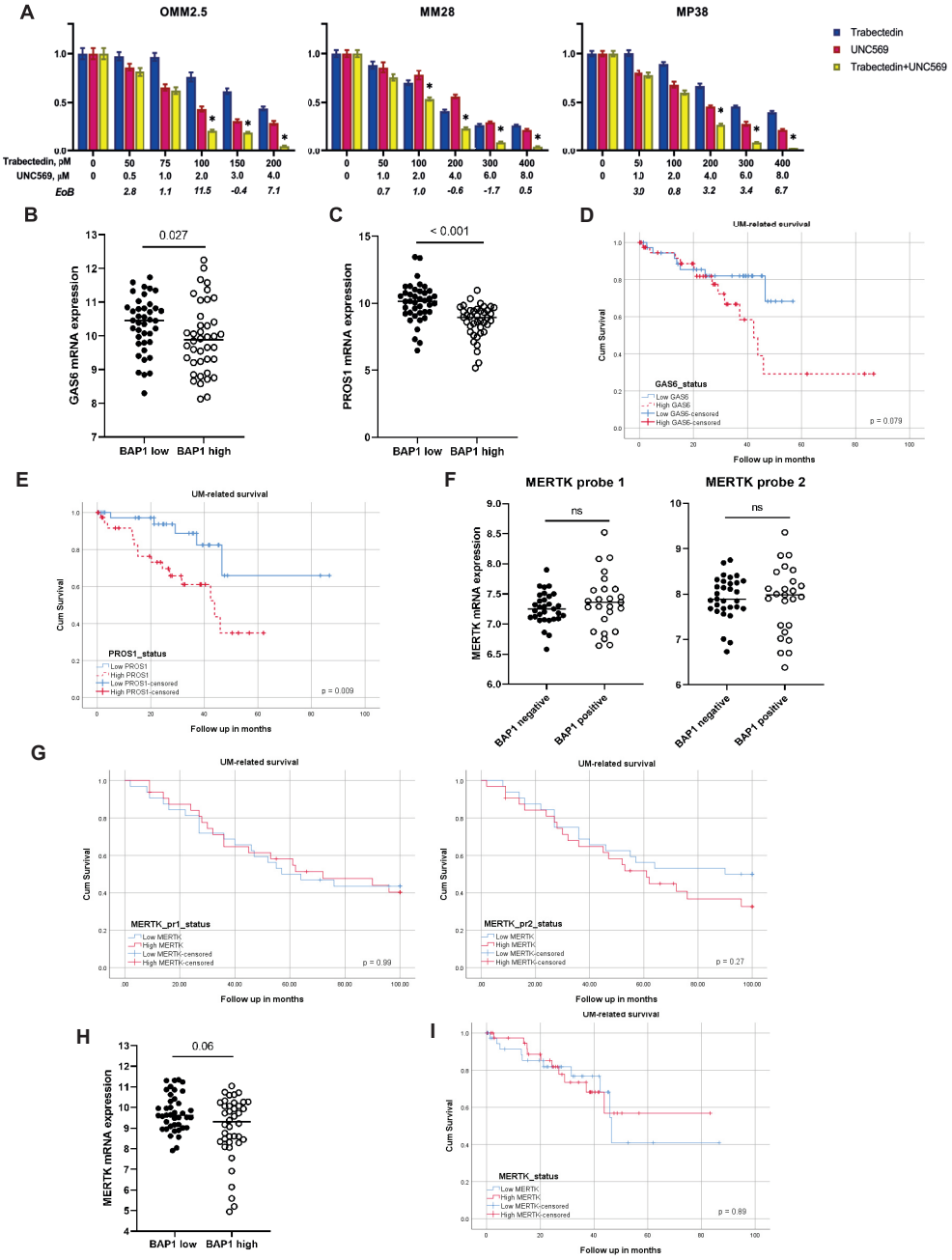

Supplementary figure 3. Analysis of TCGA uveal melanoma dataset. (A) The effect of Trabectedin (blue bars), UNC569 (magenta) and their combination (yellow) on viability of OMM2.5, MM28, MP38 cells after 5 days of treatment. Significant ($p<0.05$) reduction of viability in combinational treatment comparing to both of the single treatments is indicated with (*), statistical analysis was performed using one-way ANOVA, error bars present mean ± SEM, n=3. **(B-C)** Correlation of *GAS6* **(B)** and *PROS1***(C)** mRNA expression with BAP1 status of the tumors in TCGA cohort. **(D-E)** Analysis of the UM-specific survival correlated with *GAS6* **(D)** and *PROS1* **(E)** expression in TCGA patient cohort (n=80; split at the median, n=40 high, n=40 low).

< Supplementary figure 3. (continued) **(F)** Correlation of *MERTK* mRNA expression with BAP1 status of the tumors in LUMC cohort. Left plot represents probe 1, right plot- probe 2. **(G)** Analysis of the UM-specific survival related to *MERTK* expression in LUMC patient cohort (n=64; split at the median, n=32 high, n=32 low). **(H)** Correlation of *MERTK* mRNA expression with BAP1 status of the tumors in TCGA cohort. **(I)** Analysis of the UM-specific survival related to *MERTK* expression in TCGA patient cohort (n=80; split at the median, n=40 high, n=40 low).

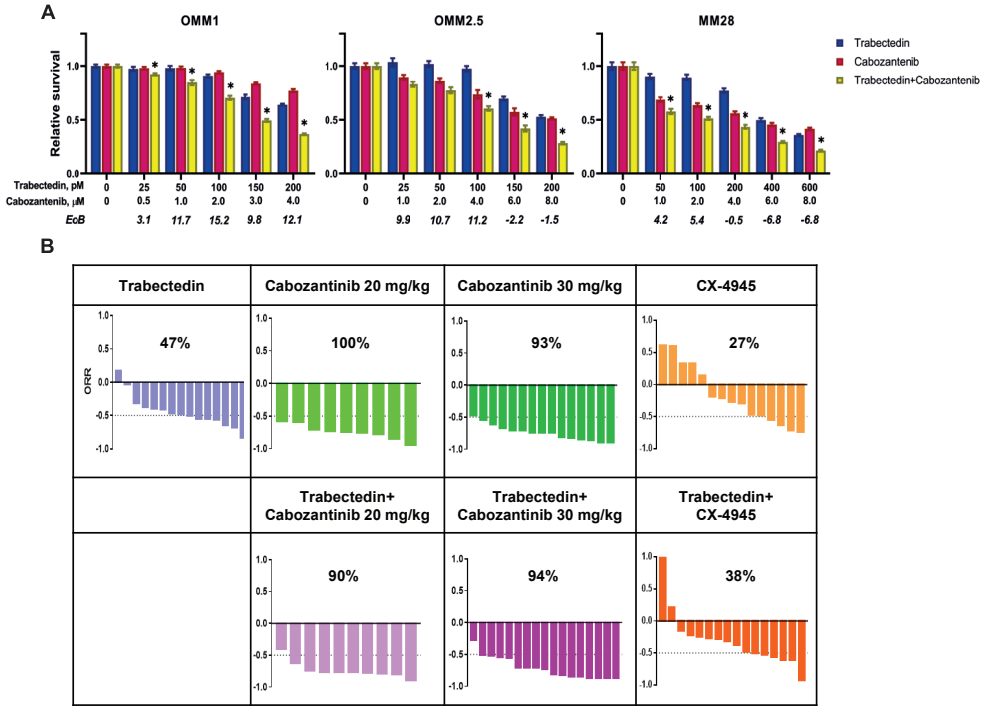

Supplementary figure 4. Overall response rate of the selected combinations. **(A)** The effect of Trabectedin (blue bars), Cabozantinib (magenta) and their combination (yellow) on viability of OMM1, OMM2.5 and MM28 cells after 5 days of treatment. Significant ($p<0.05$) reduction of viability in combinational treatment comparing to both of the single treatments is indicated with (*), statistical analysis was performed using one-way ANOVA, error bars present mean ± SEM, n=3. **(B)** Overall response rate (ORR) to Trabectedin at 0.125 mg/kg, IV, weekly, with or without 2 doses of Cabozantinib, 20 or 30 mg/kg, 5 days per week, PO, for all PDX models.

Supplementary tables

Supplementary Table 1. Sequences of i-shRNAs.

i-shRNA	Sequence
Control#1	GAATCTTGTTACATCAGCT
Control#2	TACAACAGCCACAACGTCTAT
MERTK #1	CCTGCATACTTACTTACTTTA
MERTK #2	GCTCAATCAGTGTACCTAATA
TYRO3 #1	CCGGTCCTTCAATCGAGAAAG
TYRO3 #2	CCAGTGACTGTCGGTACATAC
TYRO3 #3	TTGGTATCTCAGGTCTGAATC

Supplementary Table 2. Concentrations of compounds applied for caspase 3/7 activity assay.

Cell line	CX-4945, μM	Trabectedin, pM	Foretinib, μM
OMM1	2	200	0.5
OMM2.5	1	150	0.5
MP38	5	600	4
MP46	3	600	1.5
MM66	7	250	1

Supplementary Table 3. Concentrations of compounds applied for protein and mRNA analysis.

Cell line	CX-4945, μM	Trabectedin, pM	Foretinib, μM
OMM1	2	200	0.5
OMM2.5	1	200	0.5
MP38	5	600	2
MP46	3	600	1.5
MM66	7	300	1

Supplementary Table 4. Primary antibodies

Antibody	Ordering number	Manufacturer
AKT	#2920	Cell Signaling Technology Beverly, MA, USA
pS129-AKT	#13461	
pS473-AKT	#4060	
pT308-AKT	#13038	
cMET	#4560	
pY1234-cMET	#3126	
ERK1/2	#4695	
MERTK	#4319	
TYRO3	#5585	
pS15-P53	#9284	
PARP	#9542	
PRAS40	#2610	
pT246-PRAS40	#2640	
pT202/pY204-ERK	M8159	Sigma-Aldrich, St Louis, MO, USA
pY749/681-MERTK/Tyro3	SAB4504621	
Vinculin	V9131	
γ-Tubulin	T 6199	
Mdm2	#04-1530	Millipore, Temecula, CA, USA
Mdmx	#04-1555	
p53	sc-126	Santa Cruz Biotechnology, Dallas, TX, USA
USP7	A300-0330A-M	Bethyl laboratories, Montgomery, TX, USA

Supplementary Table 5. Concentrations of compounds applied for cell cycle analysis by flow cytometry.

Cell line	CX-4945, μM	Trabectedin, pM	Foretinib, μM
OMM1	2	200	0.5
OMM2.5	1	200	0.5
MP38	5	600	2
MP46	3	600	1.5
MM66	7	300	1

Supplementary Table 6. Primers for qPCR.

Primer	Sequence
Bcl-2 FW	CCCGCGACTCCTGATTCATT
Bcl2-RV	AGTCTACTTCCTCTGTGATGTTGT
Bim FW	CATCGCGGTATTCGGTTC
Bim RV	GCTTTGCCATTTGGTCTTTTT
Bmf FW	TTTATGGCAATGCTGGCTATCG
Bmf FW	GCAATCTGTACCTCTGCTTGATG
Mdm2 FW	ACGCACGCCACTTTTTCTCT
Mdm2 RV	TCCGAAGCTGGAATCTGTGAG
CDKN1A FW	CCTGACAGATTTCTATCACTCCA
CDKN1A RV	AGGCAGCGTATATCAGGAG

Supplementary Table 7. Primers for PCR.

Primer	Sequence
Ell FW	CTAAATCCGTCTCAGAATGCTGCAG
Ell RV	TAATCTGGGAGTTCAATTGCTGAAGG
Mdmx FW	TGCATGCAGCAGGTGCG
Mdmx RV	CATTACTTCTAGGTGTAT
Gapdh FW	AATCCCATCACCATCTTCC
Gapdh RV	ATGAGTCCTTCCACGATACC

2